

# A high-order compact finite difference scheme and precise integration method based on modified Hopf-Cole transformation for numerical simulation of n-dimensional Burgers' system

Changkai Chen<sup>a</sup>, Xiaohua Zhang<sup>a,b,\*</sup>, Zhang Liu<sup>a</sup>

<sup>a</sup>College of Science, China Three Gorges University, Yichang, 443002, China

<sup>b</sup>Three Gorges Mathematical Research Center, China Three Gorges University, Yichang, 443002, China

---

## Abstract

This paper introduces a modification of n-dimensional Hopf-Cole transformation to the n-dimensional Burgers' system. We obtain the n-dimensional heat conduction equation through the modification of the Hopf-Cole transformation. Then the high-order exponential time differencing precise integration method (PIM) based on fourth-order Taylor approximation in combination with a spatially global sixth-order compact finite difference (CFD) scheme is presented to solve the equation with high accuracy. Moreover, coupling with the Strang splitting method, the scheme is extended to multi-dimensional (two,three-dimensional) Burgers' system, which also possesses high computational efficiency and accuracy. Several numerical examples verify the performance and capability of the proposed scheme. Numerical results show that the proposed method appreciably improves the computational accuracy compared with the existing numerical method. In addition, the two-dimensional and three-dimensional examples demonstrate excellent adaptability, and the numerical simulation results also have very high accuracy in medium Reynolds numbers.

**Keywords:** n-dimensional Hopf-Cole transformation, n-dimensional Burgers' system, compact finite difference, precise integration method, Strang splitting

---

\*Corresponding author.  
E-mail addresses: zhangxiaohua07@163.com;

## 1. Introduction

Burgers' equation is a nonlinear partial differential equations (PDEs) which was first introduced by Bateman [1], and was later treated as the turbulence of the mathematical model [2, 3]. Burgers' equation is an especially important PDEs in fluid mechanics, which combines the characteristics of the first order wave equation and heat conduction equation. Burgers' equation is used as a tool to describe the interaction between convection and diffusion. Over the decades, Burgers' equation has a large variety of applications in the modeling of water in dynamic soil water, surface disturbances electromagnetic waves, density waves, statistics of flow problems, mixing and turbulent diffusion, cosmology and seismology [4, 5], etc. Hopf [6] and Cole [7] showed independently that for any given initial conditions the Burgers' equation can be reduced to a linear homogeneous heat equation that can be solved analytically and the analytical solution of the original Burgers' equation can be expressed in the form of Fourier series. Even though the analytical solution is available in the form of the Fourier series, accurate and efficient numerical schemes are still required to solve the Burgers' equation which consists of multi-dimensional system or the complex initial condition. In such situations, the Fourier series solutions for the practical applications are very limited, which converges slowly or diverges in many cases. The analytical or numerical solutions are essential for the corresponding Burgers' equations. Apart from the limited number of these problems, most of them do not have exact analytical solutions, so it is imperative to get a satisfactory solution of Burgers' equation. Here, we first analyze one-dimensional coupled Burgers' equation. Owing to the nonlinear convection term and viscous term, the coupled Burgers' equation can be studied as a simple example of the Navier-Stokes equation.

- The one-dimensional coupled nonlinear Burgers' equation [8]

$$\begin{cases} \frac{\partial u_1}{\partial t} = \omega_1 \frac{\partial^2 u_1}{\partial x^2} - \kappa_1 u_1 \frac{\partial u_1}{\partial x} - \delta_1 \frac{\partial(u_1 u_2)}{\partial x} \\ \frac{\partial u_2}{\partial t} = \omega_2 \frac{\partial^2 u_2}{\partial x^2} - \kappa_2 u_2 \frac{\partial u_2}{\partial x} - \delta_2 \frac{\partial(u_1 u_2)}{\partial x} \end{cases}, \quad x \in \Omega, \quad t \in [0, T] \quad (1)$$

subject to the initial conditions:

$$\begin{aligned} u_1(x, 0) &= g_1(t), \quad x \in \Omega = [0, l] \\ u_2(x, 0) &= g_2(t), \quad x \in \Omega = [0, l] \end{aligned} \quad (2)$$

and boundary conditions

$$\begin{aligned} u_1(a, t) &= f_1(x), \quad u_1(b, t) = f_2(x), \quad x \in \Omega = [0, l], \quad t \in [0, T] \\ u_2(a, t) &= f_3(x), \quad u_2(b, t) = f_4(x), \quad x \in \Omega = [0, l], \quad t \in [0, T] \end{aligned} \quad (3)$$

where  $\omega_1, \omega_2$  is kinematic viscosity parameters of the fluid, which correspond to an inverse of Reynolds number  $Re$  (if  $\omega_1 = \omega_2$ , then  $\omega_1 = \omega_2 = \frac{1}{Re}$ ).  $\kappa_1, \kappa_2$  are real constants and  $\delta_1, \delta_2$  are arbitrary constants.  $f(x)$  and  $g(t)$  are given smooth functions.

It is pervasively acknowledged that the nonlinear coupled Burgers' equation (1) does not have precise analytic solutions. Researchers are interested in using various numerical techniques to study the properties of Burgers' equation, because it has wide applicability in various fields of science and engineering. Due to the existence of nonlinear terms and viscosity parameters, numerical approximation of nonlinear coupled Burgers' equation is a challenging task. In Burgers' equation, discontinuities may appear in finite time, even if the initial condition is smooth. They give rise to the phenomenon of shock waves which have important applications in physics [9, 10]. Recently, some contributions related to the time-dependent coupled viscous Burgers' equation have been published, which analyze the theoretical and numerical aspects. Several numerical experiments on non-coupled and coupled Burgers' equation were run to compare the accuracy of the proposed schemes with other existing methods [11, 12, 13, 14, 15]. For the sake of clarity, a brief description of the comparison method is provided below.

Bhatt et al. [11] proposed A-stable and L-stable Fourth-order exponential time difference Runge-Kutta schemes in combination with a global fourth-order

CFD scheme for the numerical solution of the coupled Burgers' equations.

In Ref. [12], the analytical solutions of two-dimensional and three-dimensional Burgers' equations are derived. For multi-dimensional problems, these solutions can describe the shock wave phenomenon in large Reynolds numbers ( $Re \geq 100$ ), which is very useful for testing analytical solutions of numerical methods.

In Ref. [13] the author developed a Chebyshev spectral collocation method for solving approximate solutions of nonlinear PDEs. Using Chebyshev spectral collocation method, this problem is reduced to a set of ordinary differential equations (ODEs), and then solved with Runge-Kutta fourth-order method.

In Ref. [14] the author uses cubic B-spline function to construct a collocation method for numerical simulation of coupled Burgers' equation. The time derivative term is discretized by the conventional Crank-Nicolson (C-N) scheme, while the space derivative term is discretized by the cubic B-spline method. The results obtained by finite difference cubic B-spline show that the accuracy of the solution decreases with the increase of time due to the time truncation error of the time derivative term.

Jaradat et al. [15] establish new two-mode coupled Burgers' equations which are introduced for the first time. The authors find the necessary conditions in which the multiple kink and multiple singular kink solutions exist and present the two-front solutions.

In this paper, we mainly discuss the numerical scheme of n-dimensional Burgers' system. The n-dimensional Burgers' system includes non-coupled and coupled problems, and multi-dimensional problems are for coupled Burgers' equations.

- The n-dimensional Burgers' system [16, 17, 18]

$$\mathbf{U}_t + \kappa(\mathbf{U} \cdot \nabla)\mathbf{U} = \omega \Delta \mathbf{U} \quad (4)$$

where  $\mathbf{U} = (u_1, u_2, \dots, u_n)^T$  is the fluid velocity fields,  $n$  is dimension of space,  $\omega$  is the kinematic viscosity of the fluid and  $\kappa$  are real constants.  $\Delta = \frac{\partial^2}{\partial x_1^2} +$

$\frac{\partial^2}{\partial x_2^2} + \cdots + \frac{\partial^2}{\partial x_n^2}$  denotes the Laplace operator, and  $\nabla = (\frac{\partial}{\partial x_1}, \frac{\partial}{\partial x_2}, \cdots, \frac{\partial}{\partial x_n})^T$  is the Hamilton gradient operator.

The system of Eq. (4) is Burgers' equations which includes non-coupled( $n = 1$ ) and coupled( $n > 1$ ) problems. When  $n = 1, 2, 3$  and  $\kappa = 1$ , the system of Eq.(4) respectively becomes one-dimensional, two-dimensional and three-dimensional Burgers' equation

$$u_t + uu_x = \omega u_{xx} \quad (5)$$

$$\begin{aligned} u_t + uu_x + vu_y &= \omega(u_{xx} + u_{yy}) \\ v_t + uv_x + vv_y &= \omega(v_{xx} + v_{yy}) \end{aligned} \quad (6)$$

$$\begin{aligned} u_t + uu_x + vu_y + wu_z &= \omega(u_{xx} + u_{yy} + u_{zz}) \\ v_t + uv_x + vv_y + wv_z &= \omega(v_{xx} + v_{yy} + v_{zz}) \\ w_t + uw_x + vw_y + ww_z &= \omega(w_{xx} + w_{yy} + w_{zz}) \end{aligned} \quad (7)$$

Chen et al. [17] show an n-dimensional Hopf-Cole transformation between the n-dimensional Burgers' system and an n-dimensional heat equation under an irrotational condition. Motivated by this idea, the purpose of this paper is to intend to extend the Hopf-Cole transformation to linearize the n-dimensional Burgers' equation (4); After obtaining the n-dimensional heat conduction equation, the CFD scheme with high precision and high efficiency is used to solve it.

Currently, there are many numerical methods for heat conduction equation [19, 20], such as finite difference method (FDM), finite element method (FEM), finite volume method (FVM) and spectrum method, etc. The traditional FDM shows great limitations in accuracy. An important measure to improve the accuracy of the traditional FDM is to refine mesh, which in turn will increase the amount of storage and calculating speed, especially in high-dimensional cases. Therefore, it is of great theoretical significance and practical value to construct a scheme with high accuracy and excellent stability in time and space.

The CFD scheme is one of the most studied FDM at present. Experience proves that the compact scheme is much more accurate than the corresponding

explicit scheme of the same order [21]. Over the past three decades, the methods for developing high-order CFD scheme have made great progress. Dennis et. al. proposed the fourth-order CFD scheme for convection-diffusion problems [22], this scheme can get more accurate results with a thicker grid. Lele [23] developed CFD scheme with pseudo spectral resolution on the basis of summarizing the previous work and proposed a linear sixth-order central CFD scheme, which can achieve the accuracy of the spectral method. Subsequently, many scholars constructed different schemes of CFD scheme and solved many types of partial differential equations [24, 25, 26, 27], such as integro-differential equations, three-dimensional Poisson equations, the shallow water equations, and the Helmholtz equations, they all achieved better numerical results. Sengupta et. al. developed a class of upwind compact difference schemes, and such schemes could be applied to different fields [28]. In that same year, Kumar [29] discussed a high-order compact difference scheme for singularly perturbed reaction diffusion problems on a new Shish Kin mesh. Sen [30, 31] discussed the fourth-order exact compact difference scheme for mixed derivative parabolic problems with variable coefficients.

The CFD scheme is a widely used method for spatial discretization of heat conduction equations to obtain the ODEs, and then other methods of time discretization are used for discretizing the ODEs, such as Euler method, multi-step methods and Runge-Kutta method. The exact solution of heat conduction equation contains the calculation of exponential matrix. How to accurately calculate the exponential matrices is an essential problem in solving PDEs. Moler et al. [32] summarized nineteen schemes for calculating the exponential matrices. These nineteen schemes are aimed at different practical problems, and their numerical solutions also have corresponding advantages and disadvantages. In 1994, Zhong [33] proposed the precise integration method (PIM) of exponential matrices to solve the initial value problem of linear ODEs. PIM is an approximated method to calculate the exponential matrices, which contains Taylor approximation and Padé approximation. The PIM avoided the computer error caused by fine division and improved the numerical solution of exponential

matrices by the accuracy of the computation.

Alternating Direction Implicit (ADI) method is a classical numerical scheme for solving multi-dimensional heat conduction equation. ADI, such as Peacemen-Rachford scheme, D'Yakonov scheme and Douglas scheme, are only the second-order accuracy schemes [34, 35, 36]. ADI often fail to meet the accuracy requirements of practical problems. Strang splitting method (SSM) is a numerical method for solving differential equations that are decomposable into a sum of differential operators, which is to solve multi-dimensional PDEs by reducing their dimensionality to a sum of one-dimensional problems [37]. This is a scheme of operator splitting method. If the differential operators of the SSM commute, then it will lead to no loss of accuracy. Therefore, the proposed schemes will extend to multi-dimensional heat conduction equation through SSM.

The remainder of the paper is arranged as follows. The n-dimensional Hopf-Cole transformation between the n-dimensional Burgers' system and n-dimensional heat conduction equation are presented in Section 2; Moreover, we give the modification of the Hopf-Cole transformation. The high-order exponential time differencing PIM in combination with a spatially global sixth-order CFD scheme for solving n-dimensional heat conduction equations are presented in Section 3. In Section 4, the Strang splitting method is described and the proposed schemes are extended to multi-dimensional problems. In Section 5, numerical examples are carried out to test the accuracy and adaptability of the proposed schemes. The conclusions are drawn in Section 6.

## 2. n-dimensional Hopf-Cloe transformation

The purpose of n-dimensional Hopf-Cole transformation is to convert Eq. (4) into n-dimensional heat equation

$$\Phi_t - \omega \Delta \Phi_{xx} = 0 \quad (8)$$

by the n-dimensional Hopf-Cole transformation

$$U = -2\frac{\omega}{\kappa}\partial_x \ln \Phi = -2\frac{\omega}{\kappa}\frac{\Phi_x}{\Phi} \quad (9)$$

where  $\Phi = \Phi(\mathbf{x}, t)$ ,  $\mathbf{x} = (x_1, x_2, \dots, x_n)$ .

When  $n = 1, 2, 3$  and  $\kappa = 1$ , the system of Eq. (8) respectively becomes one-dimensional, two-dimensional and three-dimensional heat equations

$$\phi_t - \omega \Delta \phi_{xx} = 0 \quad (10)$$

$$\phi_t - \omega \Delta (\phi_{xx} + \phi_{yy}) = 0 \quad (11)$$

$$\phi_t - \omega \Delta (\phi_{xx} + \phi_{yy} + \phi_{zz}) = 0 \quad (12)$$

The initial and boundary conditions are

$$\Phi(\mathbf{x}, 0) = \exp\left(\int_0^{\mathbf{x}} -\frac{\mathbf{u}(\xi, 0)}{2\omega} d\xi\right), \quad \mathbf{x} \in \Omega = [a, b] \quad (13)$$

$$\Phi_{\mathbf{x}}(a, t) = \Phi_{\mathbf{x}}(b, t) = 0, \quad t \in [0, T] \quad (14)$$

### 2.1. the modification of Hopf-Cole transformation

Based on this method, we intend to extend Hopf-Cole transformation to n-dimensional Burgers' system. Assuming that the n-dimensional heat conduction equation has the irrotational condition

$$\nabla \times \mathbf{U} = \sum_{i,j=1}^n \left( \frac{\partial u_j}{\partial x_i} - \frac{\partial u_i}{\partial x_j} \right) e_i \wedge e_j = 0 \quad (15)$$

where  $e_i, e_j$  are the basis of n-dimensional Euclidean space.

To facilitate readers to understand the derivation process, Eqs. (4) and (15) can be written as the following scalar forms

$$\frac{\partial u_i}{\partial t} + \sum_{j=1}^n u_j \frac{\partial u_i}{\partial x_j} = \omega \Delta u_i, \quad i = 1, 2, \dots, n \quad (16)$$

$$\frac{\partial u_i}{\partial x_j} = \frac{\partial u_j}{\partial x_i}, \quad i, j = 1, 2, \dots, n \quad (i \neq j) \quad (17)$$



Let  $u_i = \frac{\partial \varphi}{\partial x_i}$ , substituting in Eq. (16), we obtain

$$\frac{\partial^2 \varphi}{\partial x_j \partial t} + \kappa \sum_{j=1}^n \frac{\partial \varphi}{\partial x_j} \frac{\partial^2 \varphi}{\partial x_i \partial x_j} - \omega \frac{\partial \Delta \varphi}{\partial x_j} = 0, \quad i = 1, 2, \dots, n \quad (18)$$

then Eq. (18) can be written as

$$\frac{\partial \varphi}{\partial t} + \frac{\kappa}{2} \sum_{j=1}^n \left( \frac{\partial \varphi}{\partial x_j} \right)^2 - \omega \Delta \varphi = 0 \quad (19)$$

Applying Hopf-Cole transformation, Eq. (19) will become the n-dimensional heat conduction equations. Introduce  $\varphi = -2\frac{\omega}{\kappa} \ln \Phi$  for the system of Eq. (4), we obtain Eq. (8). It is especially noted that  $\kappa$  disappears in Hopf-Cole transformation.

With the Development of Hopf-Cole transformation in past decades, Kadalbajoo et al. [38] proposed that the C-N scheme for Eq. (5) based on Hopf-Cole transformation. They discretized the space twice with C-N scheme and central difference. Due to twice spatial dispersion in  $\Phi_{\mathbf{x}}$  of Eq. (9), the numerical solution results in loss of accuracy. In 2015, Mukundan et al. [39] present numerical techniques for Burgers' equation, which use backward difference and central difference for  $\Phi_{\mathbf{x}}$ . The accuracy of these numerical schemes will decline because of the two discretizations of  $\Phi_{\mathbf{x}}$ . We have improved Hopf-Cole transformation, which will only be one dispersed in space. Firstly, Eq. (18) can be written as

$$\frac{\partial \varphi_x}{\partial t} + \frac{\kappa}{2} \sum_{j=1}^N \left( \frac{\partial \varphi_x}{\partial x_j} \right)^2 - \omega \Delta \varphi_x = 0 \quad (20)$$

Substituting  $\varphi = -\frac{\omega}{\kappa} \ln \Phi_{\mathbf{x}}$  into Eq. (20)

$$\frac{\partial \Phi_{\mathbf{x}}}{\partial t} - \omega \Delta \Phi_{\mathbf{x}} = 0 \quad (21)$$

Then the solution of Eq. (21) can be obtained utilizing high precision numerical schemes such as CFD scheme. Thus, Eq. (21) will get  $\Phi_{\mathbf{x}}$  after a spatial discretization for n-dimensional Burgers' equations. In this way, the improvement of Hopf-Cole transformation avoids the truncation error of twice spatial difference and can obtain the higher precision the first derivative of  $\Phi(\mathbf{x}, t)$ .

## 2.2. The simplification of initial value problem

For some initial value problems, Fourier series solutions of Hopf-Cole transformation will converge very slowly, which dramatically increases the complexity of the calculation. In this subsection, we simplify the initial value condition of n-dimensional(one-dimensional, two-dimensional, three-dimensional) Burgers' equation.

### 2.2.1. one-dimensional modification

Researchers have proposed the one-dimensional Burgers' equation with the following initial and boundary condition [38, 40, 41, 42, 43]

$$\begin{aligned} u(x, 0) &= u_0(x) = \sin \pi x, \quad x \in [0, 1] \\ u(0, t) &= u(1, t) = 0, \quad t > 0 \end{aligned} \quad (22)$$

It is widely noted that the analytical solution of one-dimensional heat conduction equation can be written in the standard form of the Fourier series

$$\phi(x, t) = \sum_{\alpha=0}^{\infty} C_{\alpha} \exp(-\alpha^2 \pi^2 \omega t) \cos(\alpha \pi x) \quad (23)$$

where  $C_{\alpha}$  is Fourier coefficient.

The initial conditions of one-dimensional heat conduction equation are extracted from the Eq. (32)

$$\phi(x, 0) = \sum_{\alpha=0}^{\infty} C_{\alpha} \cos\left(\frac{\alpha \pi x}{l}\right), \quad x \in \Omega = [0, 1] \quad (24)$$

with boundary conditions

$$\phi_x(x, 0) = \phi_x(x, t) = 0, \quad t \in [0, T] \quad (25)$$

by one-dimensional Hopf-Cole transformation

$$u = -2\omega \frac{\phi_x}{\phi} \quad (26)$$

Applying the Fourier transformation to Eq. (24), we will obtain Fourier coefficient  $C_{\alpha}$

$$C_{\alpha} = A_{\alpha} B_{\alpha} \quad (27)$$

where

$$A_\alpha = \begin{cases} 1, & \text{if } \alpha = 0 \\ 2, & \text{if } \alpha \neq 0 \end{cases} \quad (28)$$

$$\begin{aligned} B_\alpha &= \int_0^1 \exp\left[-\frac{1}{2\omega} \int_0^x u_0(\zeta) d\zeta\right] dx \\ &= \exp\left(-\frac{1}{2\omega\pi}\right) \int_0^1 \exp\left(\frac{\cos \pi x}{2\omega\pi}\right) \cos(\alpha\pi x) dx \end{aligned} \quad (29)$$

The challenge of the initial value problem is to calculate the coefficient  $B_\alpha$  of the Eq. (29), which is difficult for that the single integral consisting of the exponential and trigonometric function. To simplify one-dimensional problem, the main work is to convert the calculations of  $B_\alpha$  into more efficient kind.  $B_\alpha$  can be written as

$$B_\alpha = \begin{cases} 0, & \text{if } \alpha \text{ is odd} \\ I_{(\alpha)/2}\left(\frac{1}{2\omega\pi}\right), & \text{if } \alpha \text{ is even} \end{cases} \quad (30)$$

where  $I_{(n)}(1/2\omega\pi)$  is the modified Bessel function of the first kind and of order  $n$ . In 2016, Gao et al. [12] give numerical modification of analytical solution for two and three dimensional Burgers' equation. Their modification is similar to our simplification, but Gao et al. did not provide one-dimensional case. Therefore, the following two-dimensional and three-dimensional improvements refer to the ideas put forward by Gao et al.

### 2.2.2. two-dimensional modification

For the two-dimensional Burgers' equation (6), we select the modified Bessel function of the first kind and of order  $n$  to replace Fourier coefficient under the initial condition. Considering the following initial and boundary conditions [12, 44, 45, 46]

$$\begin{aligned} u(x, y, 0) &= u_0(x, y) = \sin \pi x \cos \pi y \\ v(x, y, 0) &= v_0(x, y) = \cos \pi x \sin \pi y \\ u(0, y, t) &= u(1, y, t) = v(x, 0, t) = v(x, 1, t) = 0 \end{aligned} \quad (31)$$

where the space domain is  $(x, y) \in \Omega = [0, 1] \times [0, 1]$ , and the time domain is  $t > 0$ .

It is widely noted that the analytical solution of two-dimensional heat conduction equation can be written in the standard form of the Fourier series

$$\phi(x, y, t) = \sum_{\alpha, \beta=0}^{\infty} C_{\alpha\beta} \exp[-(\alpha^2 + \beta^2)\pi^2\omega t] \cos(\alpha\pi x) \cos(\beta\pi y) \quad (32)$$

where  $C_{\alpha\beta}$  is Fourier coefficient.

The initial conditions of two-dimensional heat conduction equation are extracted from the Eq. (32)

$$\phi(x, y, 0) = \sum_{\alpha, \beta=0}^{\infty} C_{\alpha\beta} \cos(\alpha\pi x) \cos(\beta\pi y), \quad x \in \Omega = [0, 1] \quad (33)$$

and the boundary conditions

$$\phi_x(0, y, t) = \phi_x(1, y, t) = \phi_y(x, 0, t) = \phi_y(x, 1, t) = 0 \quad (34)$$

by two-dimensional Hopf-Cole transformation

$$u = -2\omega \frac{\phi_x}{\phi}, \quad v = -2\omega \frac{\phi_y}{\phi} \quad (35)$$

Applying the Fourier transformation to Eq. (33), we will obtain Fourier coefficient  $C_{\alpha\beta}$

$$C_{\alpha\beta} = A_{\alpha\beta} B_{\alpha\beta} \quad (36)$$

where

$$A_{\alpha\beta} = \begin{cases} 1, & \text{if } \alpha = 0 \text{ and } \beta = 0 \\ 2, & \text{if } \alpha = 0 \text{ and } \beta \neq 0 \\ 2, & \text{if } \alpha \neq 0 \text{ and } \beta = 0 \\ 4, & \text{if } \alpha \neq 0 \text{ and } \beta \neq 0 \end{cases} \quad (37)$$

$$\begin{aligned} B_{\alpha\beta} &= \int_0^1 \int_0^1 \exp[-\frac{1}{2\omega} D(x, y)] dx dy \\ &= \exp(-\frac{1}{2\omega\pi}) \int_0^1 \int_0^1 \exp(\frac{\cos \pi x \cos \pi y}{2\omega\pi}) \cos(\alpha\pi x) \cos(\beta\pi y) dx dy \end{aligned} \quad (38)$$

where

$$D(x, y) = \frac{1}{2} \left\{ \int_0^x [u_0(\zeta, y) + u_0(\zeta, 0)] d\zeta + \int_0^y [v_0(x, \zeta) + v_0(0, \zeta)] d\zeta \right\} \quad (39)$$

The challenge of the initial value problem is to calculate the coefficient  $B_{\alpha\beta}$  of the Eq. (38), which is difficult for that the double integral consisting of the exponential and trigonometric function. To simplify two-dimensional problem, the main work is to convert the calculations of  $B_{\alpha\beta}$  into more efficient kind.  $B_{\alpha\beta}$  can be written as

$$B_{\alpha\beta} = \begin{cases} 0, & \text{if } \alpha + \beta \text{ is odd} \\ I_{(\alpha+\beta)/2}(\frac{1}{4\omega\pi})I_{(\alpha-\beta)/2}(\frac{1}{4\omega\pi}), & \text{if } \alpha + \beta \text{ is even} \end{cases} \quad (40)$$

where  $I_{(n)}(\frac{1}{4\omega\pi})$  is the modified Bessel function of the first kind and of order  $n$ . Gao [12] proved that Eq. (38) and Eq. (40) are equal, the scheme will get more precise and efficient analytical solution through the modification.

### 2.2.3. three-dimensional modification

Because the three-dimensional Burgers' equation is too complex, its improvement is quite different from the one-dimensional and two-dimensional ones. Considering the following initial and boundary conditions [12]

$$\begin{aligned} u(x, y, z, 0) &= \sin \pi x \cos \pi y \cos \pi z \\ v(x, y, z, 0) &= \sin \pi x \cos \pi y \cos \pi z \\ w(x, y, z, 0) &= \sin \pi x \cos \pi y \cos \pi z \end{aligned} \quad (41)$$

$$\begin{aligned} u(0, y, z, t) &= u(1, y, t) = 0 \\ v(x, 0, z, t) &= v(x, 1, t) = 0 \\ w(x, y, 0, t) &= w(x, 1, t) = 0 \end{aligned} \quad (42)$$

where the space domain is  $(x, y, z) \in \Omega = [0, 1] \times [0, 1] \times [0, 1]$ , and the time domain is  $t > 0$ .

It is widely noted that the analytical solution of three-dimensional heat conduction equation can be written in the standard form of the Fourier series

$$\phi(x, y, z, t) = \sum_{\alpha, \beta, \gamma=0}^{\infty} C_{\alpha\beta\gamma} \exp(-(\alpha^2 + \beta^2 + \gamma^2)\pi^2 \omega t) \cos(\alpha\pi x) \cos(\beta\pi y) \cos(\gamma\pi z) \quad (43)$$

where  $C_{\alpha\beta\gamma}$  is Fourier coefficient.

The initial conditions of three-dimensional heat conduction equation are extracted from the Eq. (43)

$$\phi(x, y, z, 0) = \sum_{\alpha, \beta, \gamma=0}^{\infty} C_{\alpha\beta\gamma} \cos(\alpha\pi x) \cos(\beta\pi y) \cos(\gamma\pi z) \quad (44)$$

and the boundary conditions

$$\begin{aligned} \phi_x(0, y, z, t) &= \phi_x(1, y, z, t) = 0 \\ \phi_y(x, 0, z, t) &= \phi_y(x, 1, z, t) = 0 \\ \phi_z(x, y, 0, t) &= \phi_z(x, y, 1, t) = 0 \end{aligned} \quad (45)$$

By three-dimensional Hopf-Cole transformation

$$u = -2\omega \frac{\phi_x}{\phi}, \quad v = -2\omega \frac{\phi_y}{\phi}, \quad w = -2\omega \frac{\phi_z}{\phi} \quad (46)$$

Applying the Fourier transformation to Eq. (44), we will obtain Fourier coefficient  $C_{\alpha\beta\gamma}$

$$C_{\alpha\beta\gamma} = A_{\alpha\beta\gamma} B_{\alpha\beta\gamma} \quad (47)$$

where

$$A_{\alpha\beta\gamma} = \begin{cases} 1, & \text{if } \alpha = 0 \text{ and } \beta = 0 \text{ and } \gamma = 0 \\ 2, & \text{if } \alpha \neq 0 \text{ and } \beta = 0 \text{ and } \gamma = 0 \\ 2, & \text{if } \alpha = 0 \text{ and } \beta \neq 0 \text{ and } \gamma = 0 \\ 2, & \text{if } \alpha = 0 \text{ and } \beta = 0 \text{ and } \gamma \neq 0 \\ 4, & \text{if } \alpha \neq 0 \text{ and } \beta \neq 0 \text{ and } \gamma = 0 \\ 4, & \text{if } \alpha = 0 \text{ and } \beta \neq 0 \text{ and } \gamma \neq 0 \\ 4, & \text{if } \alpha \neq 0 \text{ and } \beta = 0 \text{ and } \gamma \neq 0 \\ 8, & \text{if } \alpha \neq 0 \text{ and } \beta \neq 0 \text{ and } \gamma \neq 0 \end{cases} \quad (48)$$

$$\begin{aligned} B_{\alpha\beta\gamma} &= \int_0^1 \int_0^1 \int_0^1 \exp\left[-\frac{1}{2\omega} D(x, y, z)\right] dx dy dz \\ &= \exp\left(-\frac{1}{2\omega\pi}\right) \int_0^1 \int_0^1 \int_0^1 \exp\left(\frac{\cos \pi x \cos \pi y \cos \pi z}{2\omega\pi}\right) \cos(\alpha\pi x) \cos(\beta\pi y) \cos(\gamma\pi z) dx dy dz \end{aligned} \quad (49)$$

where

$$D(x, y, z) = \frac{1}{3} \left( \begin{aligned} & \int_0^x [u_0(\zeta, y, z) + u_0(\zeta, 0, z) + u_0(\zeta, 0, 0)] d\zeta \\ & + \int_0^y [v_0(x, \zeta, z) + v_0(x, \zeta, 0) + v_0(0, \zeta, 0)] d\zeta \\ & + \int_0^z [w_0(x, y, \zeta) + w_0(0, y, \zeta) + w_0(0, 0, \zeta)] d\zeta \end{aligned} \right) \quad (50)$$

The challenge of the initial value problem is to calculate the coefficient  $B_{\alpha\beta\gamma}$  of the Eq. (49), which is difficult for that the triple integral consisting of the exponential and trigonometric function. To simplify three-dimensional problem, the main job is to convert the calculations of  $B_{\alpha\beta\gamma}$  into more efficient kind.  $B_{\alpha\beta\gamma}$  can be written as

$$B_{\alpha\beta\gamma} = \frac{(1/8\omega\pi)^\beta}{[(\alpha+\beta)/2]![(\alpha-\beta)/2]!} \times \begin{cases} \sum_{j=1}^{(\gamma+1)/2} \mu_j \frac{(\beta+2j-2)!!}{(\beta+2j-1)!!} G, & \text{if } \alpha, \beta, \gamma \text{ are all odd} \\ \sum_{j=0}^{(\gamma)/2} \mu_j \frac{(\beta+2j-2)!!}{(\beta+2j-1)!!} G, & \text{if } \alpha, \beta, \gamma \text{ are all even} \\ 0, & \text{otherwise} \end{cases} \quad (51)$$

where  $G = {}_3F_4(\frac{\beta+1}{2}, \frac{\beta}{2} + 1, \frac{\beta}{2} + j; \frac{\beta+\alpha}{2} + 1, \frac{\beta-\alpha}{2} + 1, m + 1, \frac{\beta-\alpha}{2} + j + 1; (\frac{1}{4\omega\pi})^2)$  is the generalized hypergeometric series. Ref. [47] defines the generalized hypergeometric series

$${}_pF_q(\alpha_1, \alpha_2, \dots, \alpha_p, \beta_1, \beta_2, \dots, \beta_p; \varpi) = \sum_{s=0}^{\infty} \frac{(\alpha_1)_s (\alpha_2)_s \dots (\alpha_p)_s}{(\alpha_s)_s (\alpha_2)_s \dots (\alpha_p)_s} \frac{\varpi^s}{s!} \quad (52)$$

in which  $(a)_k$  is the Pochhammer symbol and is defined as:

$$\begin{aligned} \alpha_0 &= 1 \\ (\alpha)_k &= \alpha(\alpha+1)(\alpha+2) \dots (\alpha+k-1), k \geq 1 \end{aligned} \quad (53)$$

The coefficient  $\mu_j$  in Eq. (51) is defined by the following equation:

$$\cos(\gamma\varpi) = \begin{cases} \sum_{j=1}^{\gamma/2} \mu_j \cos^{2j-1}(\varpi), & \text{if } \gamma \text{ are even} \\ \sum_{j=1}^{(\gamma+1)/2} \mu_j \cos^{2j-1}(\varpi), & \text{if } \gamma \text{ are odd} \end{cases} \quad (54)$$

### 3. high-order numerical scheme

In this section, to solve the n-dimensional heat conduction equation obtained by Hopf-Cole transformation, we will present the sixth-order CFD scheme and the precise integration method (PIM). For simplicity, we consider one-dimensional heat conduction equation (10) with mesh size  $h = x_{i+1} - x_i$ , in which  $x_i = ih, i = 1, 2, \dots, N$ , where  $h$  is spatial step size. We firstly apply the sixth-order CFD scheme to discretization in space. If  $\phi = \phi(x_i)$  and  $\phi_i''$  represent the second derivative of  $\phi(x)$  at  $x_i$ , then an approximation of the second derivatives at interior nodes may be expressed as

$$\frac{2}{11}\phi_{i-1}'' + \phi_i'' + \frac{2}{11}\phi_i'' = \frac{3}{44h^2}(\phi_{i+2} - \phi_i + \phi_{i-2}) + \frac{12}{11h^2}(\phi_{i+1} - 2\phi_i + \phi_{i-1}) \quad (55)$$

In order to make those near-boundary points have the same order accuracy as interior nodes, they should be obtained by matching Taylor series expansions to the order of  $O(h^6)$  at boundary points 1, 2,  $N-1$  and  $N$ , hence we get the following formulae [21]

$$\begin{aligned} & \phi_1'' + \frac{126}{11}\phi_2'' \\ &= \frac{1}{h^2} \left( \frac{2077}{157}\phi_1 - \frac{2943}{110}\phi_2 + \frac{573}{44}\phi_3 + \frac{167}{99}\phi_4 - \frac{18}{11}\phi_5 + \frac{57}{110}\phi_6 - \frac{131}{1980}\phi_7 \right) \end{aligned} \quad (56)$$

$$\begin{aligned} & \frac{11}{128}\phi_1'' + \phi_2'' + \frac{11}{128}\phi_3'' \\ &= \frac{1}{h^2} \left( \frac{585}{512}\phi_1 - \frac{141}{64}\phi_2 + \frac{459}{512}\phi_3 + \frac{9}{32}\phi_4 - \frac{81}{512}\phi_5 + \frac{3}{64}\phi_6 - \frac{3}{512}\phi_7 \right) \end{aligned} \quad (57)$$

$$\begin{aligned} & \frac{11}{128}\phi_N'' + \phi_{N-1}'' + \frac{11}{128}\phi_{N-2}'' \\ &= \frac{1}{h^2} \left( \frac{585}{512}\phi_N - \frac{141}{64}\phi_{N-1} + \frac{459}{512}\phi_{N-2} + \right. \\ & \quad \left. \frac{9}{32}\phi_{N-3} - \frac{81}{512}\phi_{N-4} + \frac{3}{64}\phi_{N-5} - \frac{3}{512}\phi_{N-6} \right) \end{aligned} \quad (58)$$

$$\begin{aligned} & \frac{126}{11}\phi_{N-1}'' + \phi_N'' \\ &= \frac{1}{h^2} \left( \frac{2077}{157}\phi_N - \frac{2943}{110}\phi_{N-1} + \frac{573}{44}\phi_{N-2} + \right. \\ & \quad \left. \frac{167}{99}\phi_{N-3} - \frac{18}{11}\phi_{N-4} + \frac{57}{110}\phi_{N-5} - \frac{131}{1980}\phi_{N-6} \right) \end{aligned} \quad (59)$$

Writing Eqs. (55,56,57,58,59) in matrix form as

$$A\Phi'' = B\Phi \quad (60)$$



where

$$\mathbf{A} = \begin{bmatrix} 1 & \frac{126}{11} & & & & & \\ \frac{11}{128} & 1 & \frac{11}{128} & & & & \\ & \frac{2}{11} & 1 & \frac{2}{11} & & & \\ & & \ddots & \ddots & \ddots & & \\ & & & \frac{2}{11} & 1 & \frac{2}{11} & \\ & & & & \frac{11}{128} & 1 & \frac{11}{128} \\ & & & & & \frac{126}{11} & 1 \end{bmatrix}_{N \times N} \quad (61)$$

$$\mathbf{B} = \frac{1}{h^2} \begin{bmatrix} \frac{2077}{157} & \frac{-2943}{110} & \frac{574}{44} & \frac{167}{99} & \frac{-18}{11} & \frac{57}{110} & \frac{-131}{1980} \\ \frac{585}{512} & \frac{-141}{64} & \frac{459}{512} & \frac{9}{32} & \frac{-81}{512} & \frac{3}{64} & \frac{-3}{512} \\ \frac{3}{44} & \frac{12}{11} & \frac{-51}{22} & \frac{12}{11} & \frac{3}{44} & & \\ & \ddots & \ddots & \ddots & \ddots & \ddots & \\ & & \frac{3}{44} & \frac{12}{11} & \frac{-51}{22} & \frac{12}{11} & \frac{3}{44} \\ & & \frac{-3}{512} & \frac{3}{64} & \frac{-81}{512} & \frac{9}{32} & \frac{459}{512} & \frac{-141}{64} & \frac{585}{512} \\ & & \frac{-131}{1980} & \frac{57}{110} & \frac{-18}{11} & \frac{167}{99} & \frac{574}{44} & \frac{-2943}{110} & \frac{2077}{157} \end{bmatrix}_{N \times N} \quad (62)$$

$$\Phi = (\phi_1, \phi_2, \dots, \phi_{N-1}, \phi_N)^T \quad (63)$$

Therefore the sixth-order compact finite difference approximation of second derivatives  $\Phi''$  is given by

$$\Phi'' = \mathbf{A}^{-1} \mathbf{B} \Phi = \mathbf{H} \Phi \quad (64)$$

where  $\mathbf{H} = \mathbf{A}^{-1} \mathbf{B}$ .

### 3.1. Precise integration method

After the spatial discretization, the governing PDEs become the following ODEs

$$\frac{d\Phi}{dt} = \mathbf{H} \Phi \quad (65)$$

Giving  $\tau = t_{k+1} - t_k$  as the temporal step size, then integrating Eq. (65) directly, the following recurrence formula is obtained

$$\Phi^{k+1} = e^{\mathbf{H}\tau} \Phi^k = \mathbf{T}(\tau) \Phi^k \quad (66)$$

where  $\mathbf{T}(\tau) = e^{\mathbf{H}\tau}$  is an exponential matrix.

The present work will focus on how to compute the exponential matrix  $\mathbf{T}$  very precisely. Moler et al. [32] had discussed nineteen dubious ways to compute the exponential matrix, they pointed out that the problem of calculating exponential matrix had not been fully solved. In this paper, we apply the PIM to calculate the exponential matrix, which was proposed by Zhong et al. [33]. The PIM is a algorithm of high precision for computing exponential matrix, which avoids the computer truncation error caused by the fine division and improves the numerical accuracy of the exponential matrix. In short, PIM is a series of matrix or vector multiplication calculations. Therefore, the main problem is how to calculate the exponential matrix  $e^{\mathbf{H}\tau}$ . The precise computation of exponential matrix has two core contents [48]:

(1)The incremental part of the exponential matrix is calculated separately, rather than as a whole.

(2)The addition theorem of exponent is achieved by  $2^n$  algorithm.

Using the addition theorem for the exponential matrix  $e^{\mathbf{H}\tau}$ , the following equation is obtained

$$e^{\mathbf{H}\tau} = (e^{\mathbf{H}\Delta t})^m \quad (67)$$

where  $m$  is a relatively large positive integer. In order to ensure computational accuracy, Ref. [33] suggested  $m = 2^n, n = 20, m = 1048576$ ,  $n$  is defined as bisection order.

### 3.1.1. Taylor approximation methods

The accurate computation of  $e^{\mathbf{H}\tau}$  is a challenging problem for the numerical analysis [11, 32]. The major issue is the cancellation error arising during the direct computation of  $e^{\mathbf{H}\tau}$  for eigenvalues of  $e^{\mathbf{H}}$  close to 0. To overcome this problem and other numerical issues associated with it, many researchers have proposed different methods. This study focuses on the new technique and develops CFD scheme based on Taylor approximation of  $e^{\mathbf{H}\tau}$  in order to alleviate computational difficulties associated with them. The Taylor expansion formula

to the exponential matrix  $e^{\mathbf{H}\Delta t}$  is defined as

$$e^{\mathbf{H}\Delta t} = \sum_{j=0}^{\infty} \frac{(\mathbf{H}\Delta t)^j}{j!} \quad (68)$$

where  $\Delta t = \frac{\tau}{m}$  is an extremely short time, so the truncation error in time can be ignored, the fourth-order Taylor expansion can have high precision. Hence

$$\mathbf{T}(\Delta t) \cong \sum_{j=0}^4 \frac{(\mathbf{H}\Delta t)^j}{j!} = \mathbf{I} + \mathbf{H}\Delta t + \frac{(\mathbf{H}\Delta t)^2}{2!} + \frac{(\mathbf{H}\Delta t)^3}{3!} + \frac{(\mathbf{H}\Delta t)^4}{4!} \quad (69)$$

Because  $\tau$  is very small, it is enough to expand only the the first five terms of the series. The exponential matrix  $\mathbf{T}(\Delta t)$  departs from the unit matrix  $\mathbf{I}$  to a very small extent. Hence it should be distinguished as

$$e^{\mathbf{H}\Delta t} \cong \mathbf{I} + \mathbf{T}_a = \mathbf{I} + \mathbf{H}\Delta t + \frac{(\mathbf{H}\Delta t)^2}{2!} + \frac{(\mathbf{H}\Delta t)^3}{3!} + \frac{(\mathbf{H}\Delta t)^4}{4!} \quad (70)$$

In order to obtain exponential matrix  $\mathbf{T}(\tau)$ , we need to use  $2^n$  algorithm for the matrix  $\mathbf{T}(\Delta t)$ .

### 3.1.2. $2^n$ algorithm of the exponential matrix

PIM has the problem of complete loss of precision in the exponential additional theorem [48, 49, 50]. One of the core contents of PIM is the identity matrix  $\mathbf{I}$  cannot be directly added to the incremental matrix  $\mathbf{T}_a$  for Eq. (70). Because  $\mathbf{T}_a$  is a miniature matrix. If they add up directly,  $\mathbf{T}_a$  becomes the mantissa of  $\mathbf{I} + \mathbf{T}_a$  in the process of computer operation. Thus,  $\mathbf{T}_a$  will become an appended part and its precision will seriously drop during the round-off operation in computer arithmetic. As a matter of fact,  $\mathbf{T}_a$  is an incremental part, which must be calculated and stored separately. Therefore, we will apply  $2^n$  algorithm to calculate  $\mathbf{T}_a$ .

For computing the matrix  $\mathbf{T}(\tau) = e^{\mathbf{H}\tau}$ , Eq. (67) should be factored as

$$\mathbf{T}(\tau) = (\mathbf{I} + \mathbf{T}_a)^{2^n} = (\mathbf{I} + \mathbf{T}_a)^{2^{n-1}} \times (\mathbf{I} + \mathbf{T}_a)^{2^{n-1}} \quad (71)$$

Because  $\mathbf{T}(\alpha)$  has the following equation relation of factorization

$$\mathbf{T}_{a+1} \times \mathbf{T}_{a+1} = \mathbf{I} + (2\mathbf{T}_a + \mathbf{T}_a \times \mathbf{T}_a) \quad (72)$$

Thus, Eq. (71) can be written as

$$\mathbf{T}(\tau) = \mathbf{I} + (2\mathbf{T}_a + \mathbf{T}_a \times \mathbf{T}_a)^n \quad (73)$$

The factorization (72) should be iterated  $n$  times for  $\mathbf{T}(\tau)$ . Then,  $\mathbf{T}_a$  no longer has a small value after such an iteration circulated  $n$  times according to the following computer cycle language

$$\text{for } (a = 1 : n) \mathbf{T}_a = 2\mathbf{T}_a + \mathbf{T}_a \times \mathbf{T}_a \quad (74)$$

At the end of the  $n$  cycles, the computer stores  $\mathbf{T}_a$ . At this point,  $\mathbf{T}_a$  can be directly added to the identity matrix  $\mathbf{I}$  to obtain the exponential matrix  $\mathbf{T}(\tau)$

$$\mathbf{T}(\tau) = \mathbf{I} + \mathbf{T}_a = e^{\mathbf{H}\tau} \quad (75)$$

Therefore, the Taylor approximation of the PIM can be combined with  $2^n$  algorithm to calculate the exponential matrix  $\mathbf{T}(t)$  to obtain a high precision numerical solution  $\Phi(x, t)$ . In the same way, we can use the CFD based on PIM (CFD-PIM) to obtain the solution  $\Phi_x(x, t)$  of the first derivative of the one-dimensional heat conduction equation. According to one-dimensional Hopf-Cole transformation (26),  $\Phi(x, t)$  and  $\Phi_x(x, t)$  are submitted into Eq. (26) to get the solution  $u(x, t)$  of one-dimensional Burgers' equation.

### 3.2. Stability analysis

To study the stability of our scheme, we only consider the periodic boundary condition for simplicity.

In Eq. (64), if  $\lambda_i (i = 1, 2, \dots, N - 1)$  is the eigenvalue of matrix  $\mathbf{H}$ , then  $e^{\lambda_i \tau}$  is the eigenvalue of exponential matrix  $e^{\mathbf{H}\tau}$  with the same corresponding eigenvector  $\mathbf{x} = (x_1, x_2, \dots, x_{N-1})$ . To present that CFD-PIM scheme is unconditionally stability, we need to prove the spectral radius of matrix  $e^{\mathbf{H}\tau}$  is less than 1. To this end, the following two lemmas are needed.

**Lemma 1.** If  $\lambda_i$  is an eigenvalue of matrix  $\mathbf{H} = \mathbf{A}^{-1}\mathbf{B}$  with its corresponding eigenvector  $\mathbf{x}$ , then the eigenvalue  $\lambda_i$  is real number and  $\lambda_i \leq 0$ .

**Proof.** By the definitions of eigenvalue and eigenvector, we may write , implying that [51]. This gives

$$\mathbf{x}^T \mathbf{B} \mathbf{x} = \lambda_i \mathbf{x}^T \mathbf{A} \mathbf{x} \quad (76)$$

Here, for periodic boundary condition the matrix  $\mathbf{A}$  and  $\mathbf{B}$  are as follows

$$\mathbf{A} = \begin{bmatrix} 1 & \frac{12}{11} & & & \\ \frac{12}{11} & 1 & \frac{12}{11} & & \\ & \frac{12}{11} & \ddots & \frac{12}{11} & \\ & & \frac{12}{11} & 1 & \frac{12}{11} \\ & & & \frac{12}{11} & 1 \end{bmatrix} \quad (77)$$

$$\mathbf{B} = \frac{1}{h^2} \begin{bmatrix} \frac{-51}{22} & \frac{12}{11} & \frac{3}{44} & & & \\ \frac{12}{11} & \frac{-51}{22} & \frac{12}{11} & \frac{3}{44} & & \\ \frac{3}{44} & \frac{12}{11} & \frac{-51}{22} & \frac{12}{11} & \frac{3}{44} & \\ & \ddots & \ddots & \ddots & \ddots & \ddots \\ & & \frac{3}{44} & \frac{12}{11} & \frac{-51}{22} & \frac{12}{11} & \frac{3}{44} \\ & & & \frac{3}{44} & \frac{12}{11} & \frac{-51}{22} & \frac{12}{11} \\ & & & & \frac{3}{44} & \frac{12}{11} & \frac{-51}{22} \end{bmatrix} \quad (78)$$

Obviously, the matrix  $\mathbf{A}$  and  $\mathbf{B}$  are really symmetrical, so the eigenvalue  $\lambda_i$  is real number. Meanwhile, for arbitrary  $\mathbf{x} \neq \mathbf{0}$ , the right-hand side of the Eq. (76) is

$$\mathbf{x}^T \mathbf{A} \mathbf{x} = x_1^2 + \frac{4}{11}x_1x_2 + x_2^2 + \frac{4}{11}x_2x_3 + \cdots + \frac{4}{11}x_{N-2}x_{N-1} + x_{N-1}^2 \quad (79)$$

Using the inequality  $xy < 2(x^2 + y^2)$ , we obtain

$$\begin{aligned} \mathbf{x}^T \mathbf{A} \mathbf{x} &> x_1^2 - \frac{2}{11}(x_1^2 + x_2^2) + x_2^2 - \frac{2}{11}(x_2^2 + x_3^2) + \cdots \\ &\quad - \frac{2}{11}(x_{N-2}^2 + x_{N-1}^2) + x_{N-1}^2 \\ &> \frac{9}{11}x_1^2 + \frac{7}{11} \sum_{i=2}^{N-2} x_i^2 + \frac{9}{11}x_{N-1}^2 > 0 \end{aligned} \quad (80)$$

and the left-hand side of the Eq. (76) is

$$\begin{aligned}
& \mathbf{x}^T \mathbf{B} \mathbf{x} \\
&= \frac{-51}{22}x_1^2 + \frac{12}{11}x_1x_2 + \frac{3}{44}x_1x_3 + \frac{12}{11}x_2x_1 - \frac{51}{22}x_2^2 + \frac{12}{11}x_2x_3 + \frac{3}{44}x_3x_4 \\
&+ \frac{3}{44}x_1x_3 + \frac{12}{11}x_2x_3 - \frac{51}{22}x_3^2 + \frac{12}{11}x_3x_4 + \frac{3}{44}x_4x_5 + \cdots \\
&+ \frac{3}{44}x_{N-1}x_{N-3} + \frac{12}{11}x_{N-2}x_{N-3} - \frac{51}{22}x_{N-3}^2 + \frac{12}{11}x_{N-3}x_{N-4} \\
&+ \frac{3}{44}x_{N-4}x_{N-5} + \frac{12}{11}x_{N-1}x_{N-2} - \frac{51}{22}x_{N-2}^2 + \frac{12}{11}x_{N-2}x_{N-3} \\
&+ \frac{3}{44}x_{N-3}x_{N-4} - \frac{51}{22}x_{N-1}^2 + \frac{12}{11}x_{N-1}x_{N-2} + \frac{3}{44}x_{N-1}x_{N-3}
\end{aligned} \tag{81}$$

Similarly, using the inequality  $xy < 2(x^2 + y^2)$ , we obtain

$$\mathbf{x}^T \mathbf{B} \mathbf{x} < -\frac{29}{11}(x_1^2 + x_{N-1}^2) - \frac{65}{22}(x_2^2 + \cdots + x_{N-3}^2) - \frac{3}{11}x_{N-2}^2 < 0 \tag{82}$$

From Eqs. (80) and (82), we can see that the right-hand side of the Eq. (76) is  $\mathbf{x}^T \mathbf{A} \mathbf{x} > 0$  and the left-hand side of the Eq. (76) is  $\mathbf{x}^T \mathbf{B} \mathbf{x} < 0$ . Thus,  $\lambda_i \leq 0$ .

**Lemma 2.** Let  $\mathbf{W}$  be an arbitrary square matrix. Then for any operator matrix norm  $\|\cdot\|$ , we obtain  $\lambda_i(\mathbf{W}) \leq \|\mathbf{W}\|$ , where  $\lambda_i(\mathbf{W})$  is the spectral radius of matrix  $\mathbf{W}$  [52].

**Theorem 1.** The Taylor approximation of CFDS-PIM is unconditionally stability.

**Proof.** the Taylor series approximation of  $e^{\lambda_i \tau}$  is defined as

$$e^{\lambda_i \tau} = \sum_{j=0}^{\infty} \frac{(\lambda_i \tau)^j}{j!} \tag{83}$$

Using Lemma 1, we obtain  $\lambda_i \tau \leq 0$ , thus  $e^{\lambda_i \tau} \leq 1$ . For fourth-order Taylor series approximation of the PIM,  $e^{\lambda_i \tau} < 1$ . We use Lemma 2 to get the spectral radius of matrix  $e^{\mathbf{H} \tau}$  is less than 1 in fourth-order Taylor approximation of the PIM. Thus, the Taylor approximation of CFD-PIM scheme is unconditionally stability.

#### 4. n-dimensional numerical method

Strang splitting method (SSM) is a numerical method for solving differential equations that are decompose multi-dimensional problems into a sum of

differential operators. This method is named after Gilbert Strang. It is used to speed up calculation for problems involving operators on very different time scales, and to solve n-dimensional PEDs by reducing them to a sum of one-dimensional problems.

#### 4.1. Extensions to two-dimensional case

We consider the two-dimensional heat conduction equation (11). As a precursor to Strang splitting, Eq. (11) can be written as

$$\Phi_t = H_x \Phi + H_y \Phi \quad (84)$$

where  $H_x$  and  $H_y$  are difference operator in the  $x$  and  $y$  direction. The right side of Eq. (84) is already split into a sum  $a + b$  of relatively simple expressions. Due to one of the properties of difference operator is the distributive law of multiplication, we obtain the following equations

$$\Phi_t = (H_x + H_y) \Phi \quad (85)$$

For Eq. (85), the analytical solution to the associated initial value problem would be

$$\Phi^{k+1}(t) = e^{(H_x + H_y)t} \Phi^k \quad (86)$$

This section focuses on how to calculate the exponential matrix  $e^{(H_x + H_y)t}$ , and the calculation of  $e^{(H_x + H_y)t}$  is too complicated. Thus, we convert it into calculating the product of  $e^{H_x t}$  and  $e^{H_y t}$ , but  $e^{H_x t}$  and  $e^{H_y t}$  must satisfy the commutativity of the addition theorem

$$e^{(H_x + H_y)t} = e^{H_x t} e^{H_y t} \Leftrightarrow H_x H_y = H_y H_x \quad (87)$$

Besides, the exponentials of  $H_x$  and  $H_y$  are related to that of  $H_x + H_y$  by the Trotter product formula

$$e^{H_x + H_y} = \lim_{m \rightarrow \infty} \left( e^{H_x/m} e^{H_y/m} \right)^m \quad (88)$$

Gottlieb et al. [32] suggested that the Trotter result can be used to approximate  $e^{\mathbf{H}}$  by splitting  $\mathbf{H}$  into  $\mathbf{H}_x + \mathbf{H}_y$ , because  $m = 2^{20}$  is already very large that was proposed. Thus, we use the following approximation

$$e^{\mathbf{H}} = \left( e^{\mathbf{H}_x/m} e^{\mathbf{H}_y/m} \right)^m \quad (89)$$

This approach to calculate  $e^{\mathbf{H}}$  is of potential interest when the exponentials of  $\mathbf{H}_x$  and  $\mathbf{H}_y$  can be accurately and efficiently computed. If  $\mathbf{H}_x$  and  $\mathbf{H}_y$  commute, we rewrite Eq. (86) as follows

$$\Phi^{k+1}(t) = e^{\mathbf{H}t} \Phi^k = e^{\mathbf{H}_x t} e^{\mathbf{H}_y t} \Phi^k \quad (90)$$

Thus, the two-dimensional heat conduction equation becomes two one-dimensional problems. For each one-dimensional problem, it can be solved by the CFD-PIM scheme which introduced in Sec. 3.1.

#### 4.2. Extensions to three-dimensional case

For the three-dimensional heat conduction equation, we can also use CFD-PIM based on the SSM(CFD-PIM-SSM) to decompose it into the sum of differential operators of three one-dimensional problems. The CFD-PIM scheme can be extended to three-dimensional case (12).

As a precursor to Strang splitting, we rewrite Eq. (12) as follows

$$\Phi_t = \mathbf{H}_x \Phi + \mathbf{H}_y \Phi + \mathbf{H}_z \Phi \quad (91)$$

where  $\mathbf{H}_x$ ,  $\mathbf{H}_y$  and  $\mathbf{H}_z$  are difference operators in the  $x$ -direction,  $y$ -direction, and  $z$ -direction, respectively. The right side of Eq. (91) is already split, which become a sum  $a + b + c$ . We obtain the following equations

$$\Phi_t = (\mathbf{H}_x + \mathbf{H}_y + \mathbf{H}_z) \Phi \quad (92)$$

For Eq. (85), the analytical solution to the associated initial value problem would be

$$\Phi^{k+1}(t) = e^{(\mathbf{H}_x + \mathbf{H}_y + \mathbf{H}_z)t} \Phi^k \quad (93)$$



If  $\mathbf{H}_x$ ,  $\mathbf{H}_y$  and  $\mathbf{H}_z$  commute for Eq. (93), the analytical solution to the associated initial value problem would be

$$\Phi^{k+1}(t) = e^{\mathbf{H}t} \Phi^k = e^{\mathbf{H}_x t} e^{\mathbf{H}_y t} e^{\mathbf{H}_z t} \Phi^k \quad (94)$$

Because we apply SSM to three-dimensional case, we obtain a sum of difference operator of three one-dimensional parabolic problem, the scheme has the same accuracy as one-dimensional cases. For each one-dimensional problem, it can be solved by the CFD-PIM scheme which introduced in Sec. 3.1.

## 5. Numerical Result

**Example 1.** Consider one-dimensional Burgers' equation (5) with the following initial and boundary conditions

$$\begin{aligned} u(x, 0) &= 2\omega \frac{\pi \sin \pi x}{\varepsilon + \cos \pi x}, \quad x \in [0, 1] \\ u(0, t) &= u(1, t) = 0, \quad t > 0 \end{aligned} \quad (95)$$

and the analytical solution

$$u(x, t) = 2\omega \frac{\pi \exp(-\pi^2 \omega t) \sin(\pi x)}{\varepsilon + \exp(-\pi^2 \omega t) \cos(\pi x)}, \quad x \in [0, 1], \quad t > 0 \quad (96)$$

where  $\varepsilon > 1$  is a parameter, time step size  $\tau = 5 \times 10^{-5}$ . Figs. 1,2 give the numerical solutions for different values of  $Re$  or  $\omega$ , and Tables 1,2,3 present the  $L_2$  and  $L_\infty$  of the errors at different values of  $Re$ . The results of the numerical solution are compared with those of Refs. [40, 41, 53], and CFD-PIM-SMM scheme based on Hopf-Cole transformation are better than their results. The physical behavior of the numerical solution described in Figs. 1,2 is coincident with that given in Refs. [40, 41, 53]. The solutions and the errors between the numerical solutions and the analytical solutions for large Reynolds numbers ( $Re \geq 1000$ ), which are presented in Figs. 3,4. In the left-hand side Figs. 3,4, it is obviously noted that the numerical solutions are in very good agreement with the analytical solutions. Moreover, the numerical solutions obtained by  $Re = 10^3$  and  $Re = 10^6$  have high accuracy.

Table 1: Comparison of  $L_\infty$  and  $L_2$  of the different  $Re$  with  $\varepsilon = 2$  and time  $t = 0.1$  for Example 1.

| $Re$   | Ref.[40]    |             | proposed scheme |             |
|--------|-------------|-------------|-----------------|-------------|
|        | $L_\infty$  | $L_2$       | $L_\infty$      | $L_2$       |
| 1      | 7.35746E-04 | 7.90533E-05 | 1.16573E-12     | 7.23351E-12 |
| 2      | 1.98753E-04 | 1.9657E-05  | 4.96492E-13     | 2.91693E-12 |
| 10     | 3.55811E-06 | 3.13984E-07 | 2.43139E-14     | 1.23292E-13 |
| $10^2$ | 3.36074E-08 | 2.01489E-09 | 4.03410E-15     | 1.89990E-14 |
| $10^3$ | 1.10403E-10 | 1.17301E-12 | 1.23979E-16     | 2.54818E-16 |
| $10^5$ | 3.04507E-12 | 3.07394E-14 | 1.14519E-17     | 3.43728E-17 |

Table 2: Comparison of  $L_\infty$  and  $L_2$  errors with the following numerical methods with  $Re = 200$ ,  $\varepsilon = 100$ ,  $N = 10, 20, 40, 80$ , at  $t = 1.0$  for Example 1.

| $N$ | Ref.[5]    |           | Ref.[53]   |           | proposed scheme |           |
|-----|------------|-----------|------------|-----------|-----------------|-----------|
|     | $L_\infty$ | $L_2$     | $L_\infty$ | $L_2$     | $L_\infty$      | $L_2$     |
| 10  | 1.246E-07  | 8.819E-08 | 1.215E-07  | 8.631E-08 | 4.483E-10       | 6.318E-10 |
| 20  | 3.394E-08  | 2.403E-08 | 3.062E-08  | 2.153E-08 | 2.078E-12       | 3.281E-12 |
| 40  | 1.125E-08  | 7.942E-09 | 7.644E-09  | 5.378E-09 | 5.338E-15       | 1.206E-14 |
| 80  | 5.549E-09  | 3.918E-09 | 7.644E-09  | 1.345E-09 | 4.372E-16       | 2.202E-15 |

Table 3: Comparison of  $L_\infty$  and  $L_2$  errors with the following numerical methods with  $Re = 200$ ,  $\varepsilon = 100$ ,  $N = 8, 16, 32, 64$ , at  $t = 1.0$  for Example 1

| $N$ | Ref.[41]   |           | Ref.[40]   |           | proposed scheme |           |
|-----|------------|-----------|------------|-----------|-----------------|-----------|
|     | $L_\infty$ | $L_2$     | $L_\infty$ | $L_2$     | $L_\infty$      | $L_2$     |
| 08  | 2.075E-09  | 1.278E-10 | 2.062E-09  | 1.198E-10 | 2.049E-09       | 2.874E-09 |
| 16  | 2.732E-09  | 2.183E-11 | 1.951E-09  | 2.160E-11 | 1.298E-11       | 1.934E-11 |
| 32  | 2.191E-10  | 2.734E-11 | 1.461E-10  | 1.184E-11 | 3.747E-14       | 7.227E-14 |
| 64  | 3.272E-10  | 5.852E-11 | 3.182E-10  | 2.665E-12 | 4.372E-16       | 2.202E-15 |

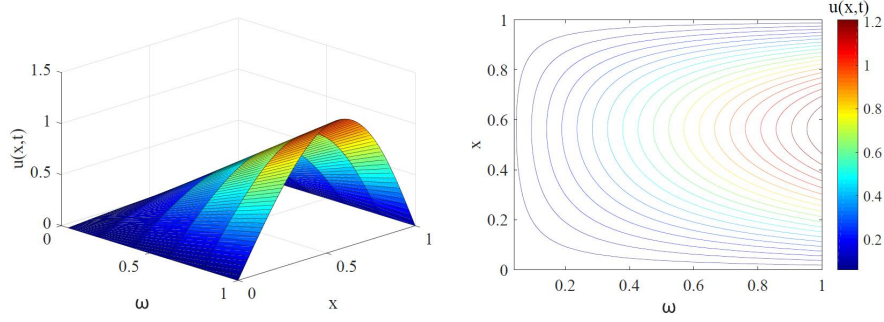


Figure 1: Physical behavior of the numerical solutions in three-dimensional figure (Left) and contour (Right) form for different values of  $\omega$  at  $t = 0.001$  with  $\varepsilon = 5$  for Example 1.

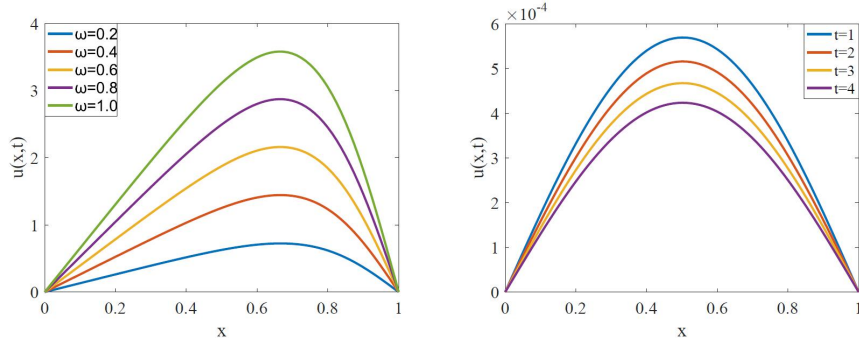


Figure 2: Physical behavior of numerical solutions with the different value of  $\omega$  and  $\varepsilon = 2$  at  $t = 0.001$  (Left); and  $t \leq 4$  with  $\omega = 0.01$ ,  $\varepsilon = 100$  (Right) for Example 1.

**Example 2.** Consider one-dimensional Burgers' equation (5) with the following initial and boundary conditions

$$\begin{aligned} u(x, 0) &= 2\omega \frac{\pi \sin \pi x + 4\pi \sin 2\pi x}{4 + \cos \pi x + 2 \cos 2\pi x}, \quad x \in [0, 1] \\ u(0, t) &= u(1, t) = 0, \quad t > 0 \end{aligned} \quad (97)$$

and the analytical solution

$$u(x, t) = 2\omega \frac{\pi \exp(-\pi^2 t) \sin \pi x + 4\pi \exp(-4\pi^2 t) \sin 2\pi x}{4 + \exp(-\pi^2 t) \cos \pi x + 2\exp(-4\pi^2 t) \cos 2\pi x} \quad (98)$$

Fig. 5 gives the numerical solutions for the different time  $t$ , and the  $L_2$  and  $L_\infty$  of the errors at different values of  $Re$  are reported in Table 4. It is observed that the numerical results show excellent agreement with the analytical

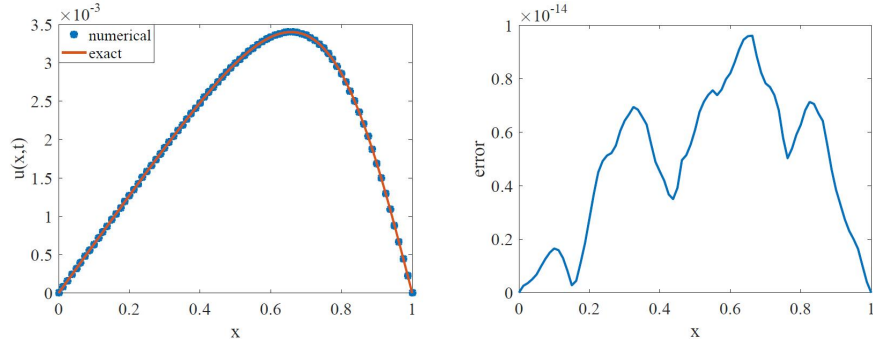


Figure 3: The numerical and exact analytical solutions (Left) and the errors between the exact analytical solutions and the numerical solutions (Right) with  $Re = 10^3$ ,  $\varepsilon = 2$  at  $t = 1$  for Example 1.

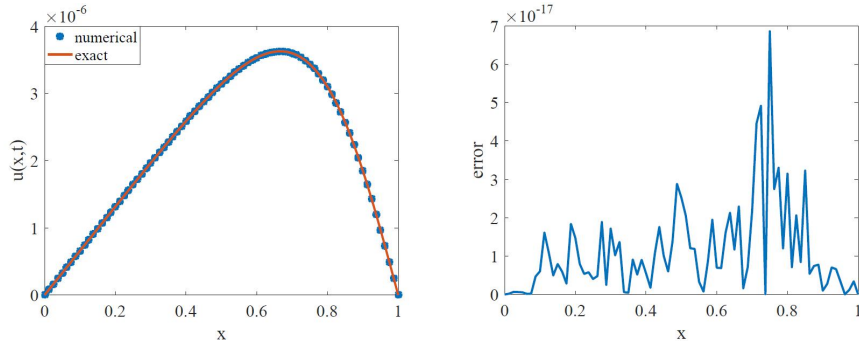


Figure 4: The numerical and exact analytical solutions (Left) and the errors between the exact analytical solutions and the numerical solutions (Right) with  $Re = 10^6$ ,  $\varepsilon = 2$  at  $t = 1$  for Example 1.

solutions. The physical behavior of the numerical solution described in Fig. 5 is coincident with that given in Ref. [54]. We observe that when  $Re$  increases,  $L_\infty$  and  $L_2$  will decrease rapidly in Table 4. The numerical simulation results present the numerical result with high accuracy in large Reynolds numbers ( $Re = 10^3$  and  $Re = 10^6$ ).

**Example 3.** To verify the effectiveness of the modified algorithm, we test the one-dimensional Burgers' equation (5) proposed in Sec. 2.2.1, over a square domain  $[0, 1]$ , with the initial and boundary conditions (22), according to one-dimensional Hopf-Cole transformation (26), the analytical(Fourier series) solu-

Table 4: Comparison of  $L_\infty$  and  $L_2$  of the different  $Re$  with  $\tau = 5 \times 10^{-4}$ , at time  $t = 0.1$  and  $t = 1.0$  for Example 2.

| $Re$   | $t = 0.1$  |            | $t = 1.0$  |             |
|--------|------------|------------|------------|-------------|
|        | $L_\infty$ | $L_2$      | $L_\infty$ | $L_2$       |
| 10     | 2.0625E-09 | 8.5343E-09 | 1.0439E-09 | 4.4330E-09  |
| $10^2$ | 2.0497E-10 | 4.1504E-10 | 1.5452E-09 | 1.89990E-09 |
| $10^3$ | 9.6175E-13 | 2.2094E-12 | 2.1661E-11 | 4.7713E-11  |
| $10^5$ | 1.9497E-16 | 4.6207E-16 | 1.8512E-15 | 4.3719E-15  |

Table 5: Comparison  $L_\infty$  and  $L_2$  errors of different  $Re$  with spatial size step  $h = 0.025$  at  $t = 0.1$  for Example 2.

| $Re$   | Ref.[53]   |          | proposed scheme |          |
|--------|------------|----------|-----------------|----------|
|        | $L_\infty$ | $L_2$    | $L_\infty$      | $L_2$    |
| 100    | 4.41E-03   | 3.55E-03 | 2.18E-10        | 4.80E-10 |
| 1000   | 4.60E-05   | 3.72E-05 | 9.63E-13        | 2.21E-12 |
| 10000  | 4.62E-07   | 3.74E-07 | 1.90E-14        | 4.38E-14 |
| 100000 | 4.62E-09   | 3.74E-09 | 2.29E-16        | 6.24E-16 |
| 100000 | 4.62E-11   | 3.74E-11 | 2.07E-17        | 5.48E-17 |

tion of Eq. (5) is

$$u(x, t) = 2\pi\omega \frac{\sum_{\alpha=0}^{\infty} \alpha C_\alpha \exp(-\alpha^2 \pi^2 \omega t) \sin(\alpha \pi x)}{\sum_{\alpha=0}^{\infty} C_\alpha \exp(-\alpha^2 \pi^2 \omega t) \cos(\alpha \pi x)} \quad (99)$$

The numerical solutions are reported in Tables 6,7,8,9 and Fig. 6 for the different values of  $Re$  and  $t$ . The results of the numerical solution are compared with those of Refs. [40, 41, 53], and the numerical results of the proposed scheme are better than their results. It is evident that the proposed scheme has high accuracy and efficiency than other numerical schemes. The left figure in Fig. 6 exhibit that as the increase of time the numerical solution of partial regions becomes steeper and steeper, and the decreasing rate of the approximate solution increases. This physical phenomenon validates the fact that the numerical solution is capable of describing the shock wave. For the numerical solutions at different time demonstrated in the left part of Fig. 6 are fantastically analogical

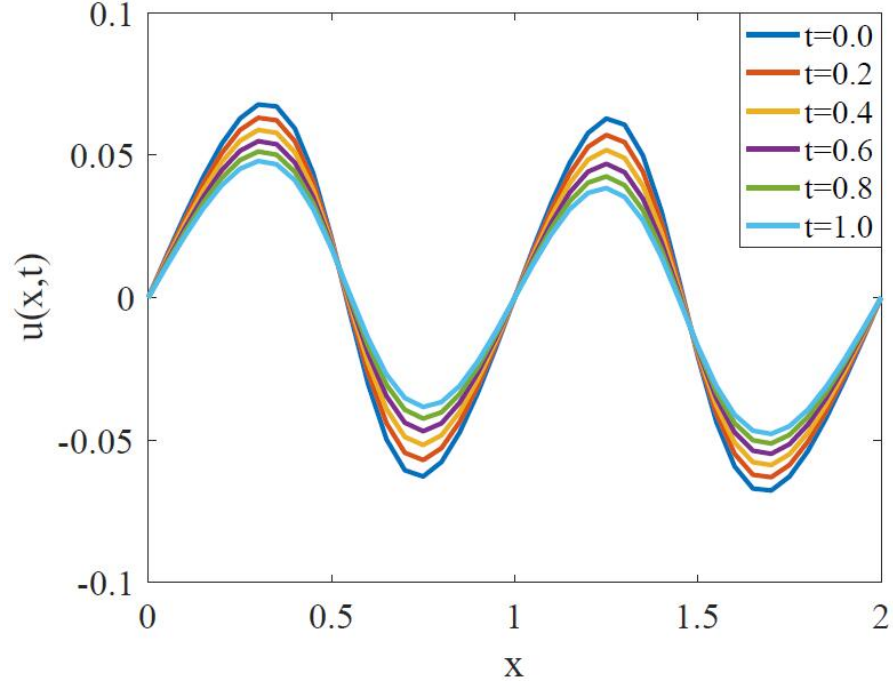


Figure 5: Numerical approximate solution of Example 2 with  $\omega = 0.01$ ,  $h = 0.05$ ,  $t \geq 1$ .

as depicted in the figures given in Refs. [40, 41, 53, 55, 43]

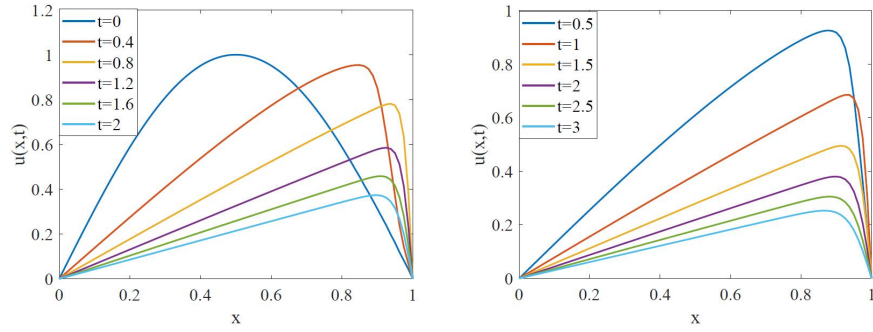


Figure 6: Physical behavior of numerical solutions at different time  $t = 0, 0.4, 0.8, 1.2, 1.6, 2.0$  for Example 3(Left) and at different time  $t = 0.5, 1.0, 1.5, 2.0, 2.5, 3.0$  for Example 4(Right)

**Example 4.** Considered the one-dimensional Burgers' equation(5) with the

Table 6: Comparison with the following numerical and analytical solutions of different values of  $x$  and  $t$  with  $Re = 10$  for Example 3.

| $x$  | $t$ | Ref.[56] | Ref.[38] | Ref.[41] | Ref.[40] | proposed scheme   | analytical solution |
|------|-----|----------|----------|----------|----------|-------------------|---------------------|
| 0.25 | 0.4 | 0.30891  | 0.30881  | 0.30887  | 0.30889  | 0.308894228585555 | 0.308894228585318   |
|      | 0.6 | 0.24075  | 0.24069  | 0.24070  | 0.24075  | 0.240739023291803 | 0.240739023291448   |
|      | 0.8 | 0.19568  | –        | 0.19566  | 0.19569  | 0.195675570103972 | 0.195675570103439   |
|      | 1.0 | 0.16257  | 0.16254  | 0.16255  | 0.16258  | 0.162564857111346 | 0.162564857110671   |
|      | 3.0 | 0.02720  | 0.02720  | 0.02721  | 0.02720  | 0.027202314473410 | 0.027202314472951   |
| 0.50 | 0.4 | 0.56964  | 0.56955  | 0.56956  | 0.56956  | 0.569632450695361 | 0.569632450693995   |
|      | 0.6 | 0.44721  | 0.44714  | 0.44715  | 0.44724  | 0.447205521200320 | 0.447205521198742   |
|      | 0.8 | 0.35924  | –        | 0.35920  | 0.35927  | 0.359236058517410 | 0.359236058515669   |
|      | 1.0 | 0.29192  | 0.29188  | 0.29188  | 0.29195  | 0.291915957127591 | 0.291915957125836   |
|      | 3.0 | 0.04021  | 0.04021  | 0.04022  | 0.04021  | 0.040204924438755 | 0.040204924438046   |
| 0.75 | 0.4 | 0.62542  | 0.62540  | 0.62540  | 0.62537  | 0.625437893711249 | 0.625437893706948   |
|      | 0.6 | 0.48721  | 0.48715  | 0.48716  | 0.48718  | 0.487214974885767 | 0.487214974882163   |
|      | 0.8 | 0.37392  | –        | 0.37389  | 0.37391  | 0.373921753212449 | 0.373921753209455   |
|      | 1.0 | 0.28748  | 0.28744  | 0.28743  | 0.28747  | 0.287474405919467 | 0.287474405916976   |
|      | 3.0 | 0.02977  | 0.02978  | 0.02978  | 0.02977  | 0.029772126859293 | 0.029772126858766   |

Table 7: Comparison with the following numerical and analytical solutions of different values of  $x$  and  $t$  with  $Re = 100$  for Example 3.

| $x$  | $t$ | Ref.[56] | Ref.[38] | Ref.[41] | Ref.[40] | proposed scheme   | analytical solution |
|------|-----|----------|----------|----------|----------|-------------------|---------------------|
| 0.25 | 0.4 | 0.34819  | 0.34229  | 0.34184  | 0.34191  | 0.341914932413026 | 0.341914932411983   |
|      | 0.6 | 0.27536  | 0.26902  | 0.26891  | 0.26896  | 0.268964845317425 | 0.268964845316620   |
|      | 0.8 | 0.22752  | –        | 0.22143  | 0.22148  | 0.221481914524793 | 0.221481914524373   |
|      | 1.0 | 0.19375  | 0.18817  | 0.18815  | 0.18820  | 0.188193961397110 | 0.188193961396738   |
|      | 3.0 | 0.07754  | 0.07511  | 0.07510  | 0.07511  | 0.075114083887341 | 0.075114083887190   |
| 0.50 | 0.4 | 0.66543  | 0.66797  | 0.66060  | 0.66069  | 0.660710972121299 | 0.660710970851541   |
|      | 0.6 | 0.53525  | 0.53211  | 0.52932  | 0.52942  | 0.529418263880240 | 0.529418263729147   |
|      | 0.8 | 0.44526  | –        | 0.43905  | 0.43914  | 0.439138250704212 | 0.374420037644682   |
|      | 1.0 | 0.38047  | 0.37500  | 0.37436  | 0.37443  | 0.374420037662816 | 0.374420037644682   |
|      | 3.0 | 0.15362  | 0.15018  | 0.15017  | 0.15019  | 0.150179005234648 | 0.150179005235832   |
| 0.75 | 0.4 | 0.91201  | 0.93680  | 0.91026  | 0.91023  | 0.910227039712648 | 0.910268136079484   |
|      | 0.6 | 0.77132  | 0.77724  | 0.76719  | 0.76723  | 0.767241968056591 | 0.767243282478514   |
|      | 0.8 | 0.65254  | –        | 0.64745  | 0.64740  | 0.647395126988680 | 0.647395234822761   |
|      | 1.0 | 0.56157  | 0.56157  | 0.55608  | 0.55606  | 0.556050682504419 | 0.556050704468246   |
|      | 3.0 | 0.22874  | 0.22485  | 0.22504  | 0.22486  | 0.224811248098947 | 0.224811248193590   |

initial and boundary conditions in the following form [40, 41, 42, 43]

$$\begin{aligned}
u(x, 0) &= 4x(1 - x), \quad x \in [0, 1] \\
u(0, t) &= u(1, t) = 0 \quad t > 0
\end{aligned} \tag{100}$$

Table 8: Comparison with the following numerical and analytical solutions of different values of  $x$  and  $t$  with  $Re = 250$  for Example 3.

| $x$  | $t$ | Ref.[41] | Ref.[40] | proposed scheme   | analytical solution |
|------|-----|----------|----------|-------------------|---------------------|
| 0.25 | 1   | 0.18886  | 0.18891  | 0.188904028952253 | 0.188904028954593   |
|      | 5   | 0.04696  | 0.04697  | 0.046972248502359 | 0.046972248504186   |
|      | 10  | 0.02421  | 0.02422  | 0.024219349937584 | 0.024219349938452   |
|      | 15  | 0.01631  | 0.01632  | 0.016315403451694 | 0.016315403452212   |
| 0.50 | 1   | 0.37591  | 0.37598  | 0.375976069095031 | 0.375976161729609   |
|      | 5   | 0.09393  | 0.09394  | 0.093937808697455 | 0.093937808702720   |
|      | 10  | 0.04843  | 0.04843  | 0.048437164796407 | 0.048437164794287   |
|      | 15  | 0.03259  | 0.03259  | 0.032594593756193 | 0.032594593752612   |
| 0.75 | 1   | 0.55875  | 0.55883  | 0.688627292675253 | 0.558832507456445   |
|      | 5   | 0.14088  | 0.14089  | 0.140886856687920 | 0.140886857891414   |
|      | 10  | 0.07221  | 0.07221  | 0.072202470037889 | 0.072202470007220   |
|      | 15  | 0.04679  | 0.04678  | 0.046775293138519 | 0.046775293123406   |

Table 9: Comparison with the following numerical and analytical solutions of different values of  $x$  and  $t$  with  $Re = 333$  ( $\omega = 0.003$ ) for Example 3.

| $x$  | $t$ | Ref.[41] | Ref.[40] | proposed scheme   | analytical solution |
|------|-----|----------|----------|-------------------|---------------------|
| 0.25 | 1   | 0.18898  | 0.18902  | 0.189018752703255 | 0.189018752707674   |
|      | 5   | 0.04697  | 0.04698  | 0.046980913294311 | 0.046980913295967   |
|      | 10  | 0.02421  | 0.02422  | 0.024221728935967 | 0.024221728937193   |
|      | 15  | 0.01631  | 0.01631  | 0.016317115629303 | 0.016317115630223   |
| 0.50 | 1   | 0.37615  | 0.37623  | 0.376221530760177 | 0.376226439382578   |
|      | 5   | 0.09394  | 0.09396  | 0.093955254104130 | 0.093955254132768   |
|      | 10  | 0.04843  | 0.04844  | 0.048442974908420 | 0.048442974906096   |
|      | 15  | 0.03263  | 0.03263  | 0.032631667278937 | 0.032631667274687   |
| 0.75 | 1   | 0.55919  | 0.55928  | 0.056946219634146 | 0.573720468311010   |
|      | 5   | 0.14091  | 0.14092  | 0.140916274868904 | 0.140916257701730   |
|      | 10  | 0.07261  | 0.07261  | 0.072602464579491 | 0.072602464234716   |
|      | 15  | 0.04840  | 0.04839  | 0.048383339743534 | 0.048383339666086   |

The analytical solution of the example is obtained by Hopf-Cole transformation and given by

$$u(x, t) = 2\pi\omega \frac{\sum_{\alpha=0}^{\infty} \alpha C_{\alpha} \exp(-\alpha^2 \pi^2 \omega t) \sin(\alpha \pi x)}{\sum_{\alpha=0}^{\infty} C_{\alpha} \exp(-\alpha^2 \pi^2 \omega t) \cos(\alpha \pi x)} \quad (101)$$

where  $C_{\alpha} = \int_0^1 \exp(-\frac{3x^2-2x^3}{3\omega}) \cos(\alpha \pi x) dx$ .

The numerical solutions are reported in Tables 10,11,12,13 and the left of



Table 10: Comparison with the following numerical and analytical solutions of different values of  $x$  and  $t$  at  $Re = 10$  for Example 4.

| $x$  | $t$ | Ref.[56] | Ref.[38] | Ref.[41] | Ref.[40] | proposed scheme    | analytical solution |
|------|-----|----------|----------|----------|----------|--------------------|---------------------|
| 0.25 | 0.4 | 0.32091  | 0.31743  | 0.30887  | 0.31752  | 0.317522880347015  | 0.317522880346768   |
|      | 0.6 | 0.24910  | 0.24609  | 0.24609  | 0.24615  | 0.246138455742101  | 0.246138455741545   |
|      | 0.8 | 0.20211  | –        | 0.19952  | 0.19957  | 0.199555307717655  | 0.199555307716945   |
|      | 1.0 | 0.16782  | 0.16558  | 0.16557  | 0.16561  | 0.165598631697920  | 0.165598631696975   |
|      | 3.0 | 0.02828  | 0.02776  | 0.02775  | 0.02776  | 0.0277587147409405 | 0.0277587147402992  |
| 0.50 | 0.4 | 0.58788  | 0.58446  | 0.56979  | 0.58454  | 0.584537259425254  | 0.584537259423137   |
|      | 0.6 | 0.46174  | 0.45791  | 0.45790  | 0.45800  | 0.457976404559216  | 0.457976404556937   |
|      | 0.8 | 0.37111  | –        | 0.36734  | 0.36744  | 0.367398193138897  | 0.367398193136396   |
|      | 1.0 | 0.30183  | 0.29831  | 0.29829  | 0.29838  | 0.298343106948955  | 0.298343106946419   |
|      | 3.0 | 0.04185  | 0.04107  | 0.04105  | 0.04107  | 0.0410649880565192 | 0.0410649880555213  |
| 0.75 | 0.4 | 0.65054  | 0.64558  | 0.62567  | 0.64556  | 0.645615507513612  | 0.645615507508048   |
|      | 0.6 | 0.50825  | 0.50261  | 0.48715  | 0.50265  | 0.502675751380125  | 0.487214974882163   |
|      | 0.8 | 0.39068  | –        | 0.38525  | 0.38532  | 0.385335518831250  | 0.385335518826972   |
|      | 1.0 | 0.30057  | 0.29582  | 0.29578  | 0.29585  | 0.295856684507498  | 0.295856684503934   |
|      | 3.0 | 0.03106  | 0.03044  | 0.03043  | 0.03044  | 0.030439645241697  | 0.0304396452409553  |

Table 11: Comparison with the following numerical and analytical solutions of different values of  $x$  and  $t$  at  $Re = 100$  for Example 4.

| $x$  | $t$ | Ref.[56] | Ref.[38] | Ref.[41] | Ref.[40] | proposed scheme    | analytical solution |
|------|-----|----------|----------|----------|----------|--------------------|---------------------|
| 0.25 | 0.4 | 0.36911  | 0.36273  | 0.36217  | 0.36225  | 0.362259376075281  | 0.362259376073489   |
|      | 0.6 | 0.28905  | 0.28212  | 0.28197  | 0.28204  | 0.282036591513099  | 0.282036591511979   |
|      | 0.8 | 0.23703  | –        | 0.23040  | 0.23045  | 0.230451149153338  | 0.230451149152527   |
|      | 1.0 | 0.20069  | 0.19467  | 0.19465  | 0.19469  | 0.194690408260556  | 0.194690408259685   |
|      | 3.0 | 0.07865  | 0.07613  | 0.07613  | 0.07613  | 0.0761340977956900 | 0.0761340977955589  |
| 0.50 | 0.4 | 0.68818  | 0.69186  | 0.68357  | 0.68364  | 0.683678602490051  | 0.683678600370378   |
|      | 0.6 | 0.55425  | 0.55125  | 0.54822  | 0.54831  | 0.548316368497342  | 0.548316368317319   |
|      | 0.8 | 0.46011  | –        | 0.45363  | 0.45371  | 0.453713562392358  | 0.453713562356646   |
|      | 1.0 | 0.39206  | 0.38627  | 0.38561  | 0.38568  | 0.385675773512666  | 0.385675773495255   |
|      | 3.0 | 0.15576  | 0.15218  | 0.15217  | 0.15219  | 0.152179982154137  | 0.152179982157813   |
| 0.75 | 0.4 | 0.92194  | 0.94940  | 0.92050  | 0.92044  | 0.920310533019500  | 0.920500316286758   |
|      | 0.6 | 0.78676  | 0.79399  | 0.78293  | 0.78297  | 0.782987516718732  | 0.782993943142911   |
|      | 0.8 | 0.66777  | –        | 0.66264  | 0.66272  | 0.662719898665532  | 0.662720379851496   |
|      | 1.0 | 0.57491  | 0.57170  | 0.56924  | 0.56932  | 0.569318600549117  | 0.569318674228527   |
|      | 3.0 | 0.23183  | 0.22778  | 0.22774  | 0.22779  | 0.227743047724488  | 0.227743047910593   |

Fig. 6 for the different values of  $Re$  and  $t$ . The results of numerical solution are compared with those of Refs. [40, 41, 53], and the outcomes of the proposed scheme are better than other numerical schemes. It can be seen that the proposed numerical scheme has high accuracy and efficiency. The right figure in

Table 12: Comparison with the following numerical and analytical solutions of different values of  $x$  and  $t$  at  $Re = 250$  for Example 4.

| $x$  | $t$ | Ref.[41] | Ref.[40] | proposed scheme     | analytical solution |
|------|-----|----------|----------|---------------------|---------------------|
| 0.25 | 1   | 0.19668  | 0.19673  | 0.196721006924063   | 0.196721006918210   |
|      | 5   | 0.04746  | 0.04747  | 0.0474646578953755  | 0.0474646578969268  |
|      | 10  | 0.02434  | 0.02434  | 0.0243496757937295  | 0.0243496757952278  |
|      | 15  | 0.01637  | 0.01637  | 0.0163750559931414  | 0.0163750559943980  |
| 0.50 | 1   | 0.38890  | 0.38898  | 0.388957541575652   | 0.388965630230683   |
|      | 5   | 0.09491  | 0.09491  | 0.0949115366085281  | 0.0949115366373159  |
|      | 10  | 0.04870  | 0.04869  | 0.0486980981880172  | 0.0486980981855498  |
|      | 15  | 0.03274  | 0.03275  | 0.0327474748053791  | 0.0327474748016372  |
| 0.75 | 1   | 0.57375  | 0.57383  | -0.0298162927259435 | 0.712326937087775   |
|      | 5   | 0.14232  | 0.14233  | 0.142323744044387   | 0.142323719655276   |
|      | 10  | 0.07298  | 0.07299  | 0.0729854327525899  | 0.0729854324288534  |
|      | 15  | 0.04857  | 0.04857  | 0.0485652950286558  | 0.0485652949610154  |

Table 13: Comparison with the following numerical and analytical solutions of different values of  $x$  and  $t$  at  $Re = 333$  ( $\omega = 0.003$ ) for Example 4.

| $x$  | $t$ | Ref.[41] | Ref.[40] | proposed scheme    | analytical solution |
|------|-----|----------|----------|--------------------|---------------------|
| 0.25 | 1   | 0.19636  | 0.19640  | 0.196393001555368  | 0.196393001558115   |
|      | 5   | 0.04744  | 0.04744  | 0.0474385758686267 | 0.0474385758702194  |
|      | 10  | 0.02434  | 0.02434  | 0.0243426312132914 | 0.0243426312140327  |
|      | 15  | 0.01637  | 0.01637  | 0.0163712480283952 | 0.0163712480286770  |
| 0.50 | 1   | 0.38842  | 0.38850  | 0.388490605742711  | 0.388490760181364   |
|      | 5   | 0.09491  | 0.09487  | 0.0948608886366821 | 0.0948608886397287  |
|      | 10  | 0.04868  | 0.04868  | 0.0486831286793741 | 0.0486831286757082  |
|      | 15  | 0.03270  | 0.03271  | 0.0327070001194449 | 0.0327070001153579  |
| 0.75 | 1   | 0.57312  | 0.57320  | 0.241682856205607  | 0.573193730672768   |
|      | 5   | 0.14224  | 0.14225  | 0.142248496442300  | 0.142248497194700   |
|      | 10  | 0.07258  | 0.07258  | 0.0725810446483559 | 0.0725810445985044  |
|      | 15  | 0.04696  | 0.04697  | 0.0469643692945623 | 0.0469643692723023  |

Fig. 6 exhibit that the numerical solution of partial regions becomes steeper and steeper over time, and the decreasing rate of the approximate solution increases. This physical phenomenon validates the fact that the numerical solution is capable of describing the shock wave. For numerical solutions in different time, the right part of Fig. 6 is quite similar as depicted in the figures given in Ref. [40, 41, 53, 55, 43].

**Example 5.** To validate the order of convergence of the proposed scheme, a numerical experiment of coupled Burgers' equation (1) was carried out in

Example 5 with the region  $x \in \Omega = [-\pi, \pi]$  with initial conditions

$$\begin{aligned} u(x, 0) &= \sin x, \quad x \in \Omega = [-\pi, \pi] \\ v(x, 0) &= \sin x, \quad x \in \Omega = [-\pi, \pi] \end{aligned} \quad (102)$$

extracted from the following exact solution given by Refs. [11, 57] for  $\omega_1 = \omega_2 = 1.0$ ,  $\kappa_1 = \kappa_2 = -2.0$ ,  $\delta_1 = \delta_2 = 1.0$ :

$$u(x, t) = v(x, t) = \exp(-t) \sin x, \quad x \in \Omega = [-\pi, \pi], t > 0 \quad (103)$$

The boundary conditions are extracted from the analytical solution (In this example,  $\tau = 4 \times 10^{-4}$ ). The spatiotemporal evolution of the numerical solution is shown in the left part of Fig. 7. To intuitively observe the physical phenomena of the example, The left figure of Fig. 7 is depicted to visually compare the analytical solutions with the numerical solutions of  $u(x, t)$  at different time  $t$ . It is observed that the numerical results show great agreement with the analytical solutions. The numerical results reflect the motion characteristics of wave propagation: the amplitude of the wave decreases with time while the wavelength remains unchanged. In addition, the errors of  $L_\infty$ , rates of convergence and CPU running time are listed in Table 14. As can be observed in Table 14, the accuracy and efficiency of our numerical scheme are much higher than that of Ref. [11] under the same spatial step size. It is observed that the error of  $L_\infty$  becomes smaller as the mesh size is refined. The computer operating environment of the algorithm is worse than that of Ref. [11], and the computation time and convergence order of our numerical scheme are much better than that of Ref. [11], which shows that the proposed scheme has excellent adaptability. The proposed scheme presents more accurate and high-efficient solutions in spatial direction than the scheme in Refs. [11, 58].

**Example 6.** To test the applicability of the proposed scheme for two-dimensional problems, we consider the two-dimensional Burgers' equations (6) over a square domain  $[0, 1] \times [0, 1]$ , with the initial conditions

$$\begin{aligned} u(x, y, 0) &= -2\omega \frac{-2\pi \cos 2\pi x \sin \pi y}{2 + \sin 2\pi x \sin \pi y} \\ v(x, y, 0) &= -2\omega \frac{-2\pi \sin \pi x \cos \pi y}{2 + \sin 2\pi x \sin \pi y} \end{aligned} \quad (104)$$

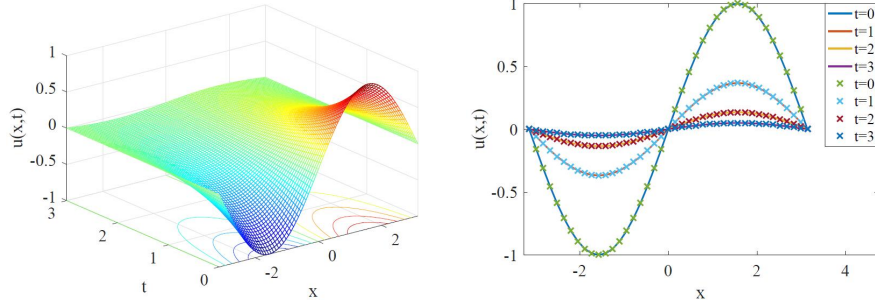


Figure 7: Evolution profile of numerical scheme at time  $T = [0, 3]$  with  $N = 41$  (Left), A comparison between numerical and analytical solutions at different time  $t$  (Right) with  $N = 41$  for Example 5. (The solid line represents the analytical solution and the other curve is the numerical solution.)

Table 14:  $L_\infty$ , rates of convergence, and CPU time of the following numerical schemes in Matlab for Example 5.

| $h$      | Ref.[11]                                 |   |        | proposed scheme                         |   |        |
|----------|--|---|--------|---|---|--------|
|          | $L_\infty$                               | $\log \frac{L_\infty(u_N)}{L_\infty(u_{2N})}$ | CPU(s) | $L_\infty$                              | $\log \frac{L_\infty(u_N)}{L_\infty(u_{2N})}$ | CPU(s) |
| $\pi/8$  | 3.660E-04                                | -   | 0.1492 | 1.149E-05                               | -   | 0.071  |
| $\pi/16$ | 2.277E-06                                | 4.0066  | 0.3109 | 2.968E-08                               | 8.8967  | 0.079  |
| $\pi/32$ | 1.422E-07                                | 4.0017  | 0.5419 | 1.329E-10                               | 7.8030  | 0.081  |
| $\pi/64$ | 8.882E-09                                | 4.0004  | 1.0726 | 1.480E-12                               | 6.4886  | 0.118  |
| platform | Intel Core i7-4510U 2.60 GHz workstation |   |        | Intel Core i5-6300HQ 2.30 GHz processor |   |        |

for which the analytical solutions [59] are

$$u(x, y, t) = 4\pi\omega \frac{\exp(-5\pi^2\omega t) \cos 2\pi x \sin \pi y}{2 + \exp(-5\pi^2\omega t) \sin 2\pi x \sin \pi y} \quad (105)$$

$$v(x, y, t) = 4\pi\omega \frac{\exp(-5\pi^2\omega t) \sin 2\pi x \cos \pi y}{2 + \exp(-5\pi^2\omega t) \sin 2\pi x \sin \pi y} \quad (106)$$

The boundary conditions are extracted from the analytical solution, and  $\tau = 5 \times 10^{-4}$ . This example uses the CFD scheme with sixth-order accuracy in space and the PIM with fourth-order accuracy in time. The numerical simulation results are shown in Table 15 and Figs. 8,9. To prove that the method is sixth-order accuracy in space, the time step  $\tau$  is fixed to  $5 \times 10^{-4}$ , thus the time truncation error can be ignored. To simplify the demonstration, we use the

same grid size in the  $x$  and  $y$  directions. As can be seen from Table 15, when  $h$  is reduced by a factor of 2, the maximal errors for both  $u(x, y, t)$  and  $v(x, y, t)$  are reduced by a factor of 6, which indicates that the method is sixth-order accurate in space. When  $h$  is reduced by a factor of 2, the  $L_\infty$  of  $u(x, y, t)$  and  $v(x, y, t)$  are both reduced by a factor of  $2^6$ , which indicates that the method is sixth-order accurate in space. Besides, The accuracy of the numerical solution of the proposed scheme is much higher than that of Ref. [59]. It is observed that the numerical solutions present excellent agreement with the analytical solutions.

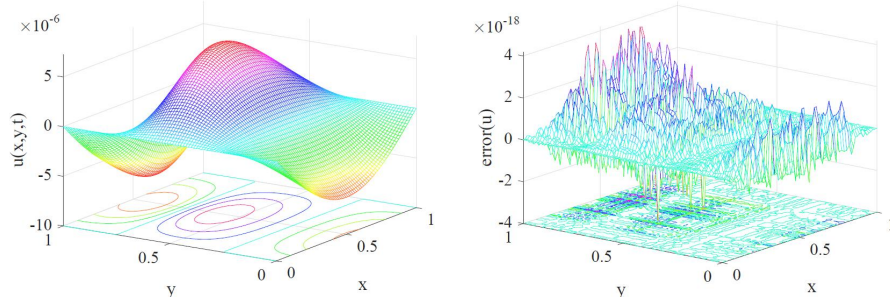


Figure 8: Physical behavior of the numerical solutions  $u(x, y, t)$  (Left), and the errors (Right) between the analytical and numerical solutions with  $Re = 10^6$  and  $N \times N = 81 \times 81$  at  $t = 1$  for Example 6.

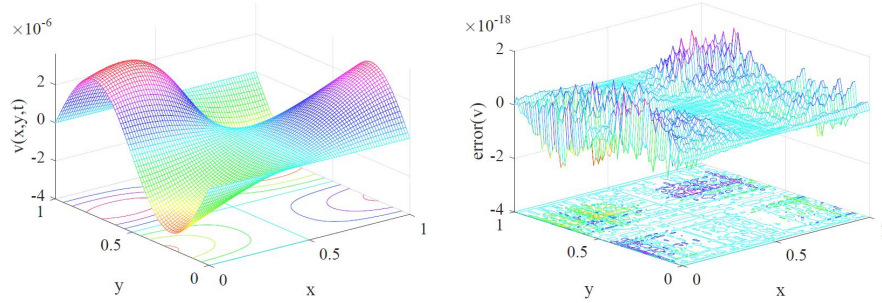


Figure 9: Physical behavior of the numerical solutions  $v(x, y, t)$  (Left), and the errors (Right) between the analytical and the numerical solutions with  $Re = 10^6$  and  $N \times N = 81 \times 81$  at  $t = 1$  for Example 6.

Table 15: Comparison of  $L_\infty$  errors of two numerical schemes in space with  $Re = 10$  at  $t = 1.0$  for Example 6.

| $N \times N$                                  | Ref.[59]       |                |                | proposed scheme |                |                |
|---|----------------|----------------|----------------|-----------------|----------------|----------------|
|   | $11 \times 11$ | $21 \times 21$ | $41 \times 41$ | $11 \times 11$  | $21 \times 21$ | $41 \times 41$ |
| $L_\infty(u)$                                 | 8.4895E-06     | 5.9972E-07     | 3.8565E-08     | 8.0255E-07      | 4.0998E-09     | 3.6063E-11     |
| $\log \frac{L_\infty(u_N)}{L_\infty(u_{2N})}$ | —              | 3.8233         | 3.9589         | —               | 7.6129         | 6.8289         |
| $L_\infty(v)$                                 | 6.8012E-06     | 4.5433E-07     | 2.8505E-08     | 1.2944E-04      | 1.1137E-06     | 5.0211E-09     |
| $\log \frac{L_\infty(v_N)}{L_\infty(v_{2N})}$ | —              | 3.9040         | 3.9944         | —               | 6.8608         | 5.4018         |

**Example 7.** In order to verify the effectiveness of the improvement proposed above, we consider the system of two-dimensional Burgers' equations (6) proposed in Sec. 2.2.2, over a square domain  $[0, 1] \times [0, 1]$ , with the initial and boundary conditions (31) and the analytical solution

$$\begin{aligned}
 u(x, y, t) &= 2\pi\omega \frac{\sum_{\alpha, \beta=0}^{\infty} \alpha C_{\alpha\beta} \exp[-(\alpha^2 + \beta^2)\pi^2\omega t] \sin(\alpha\pi x) \cos(\beta\pi y)}{\sum_{\alpha, \beta=0}^{\infty} C_{\alpha\beta} \exp[-(\alpha^2 + \beta^2)\pi^2\omega t] \cos(\alpha\pi x) \cos(\beta\pi y)} \\
 v(x, y, t) &= 2\pi\omega \frac{\sum_{\alpha, \beta=0}^{\infty} \beta C_{\alpha\beta} \exp[-(\alpha^2 + \beta^2)\pi^2\omega t] \cos(\alpha\pi x) \sin(\beta\pi y)}{\sum_{\alpha, \beta=0}^{\infty} C_{\alpha\beta} \exp[-(\alpha^2 + \beta^2)\pi^2\omega t] \cos(\alpha\pi x) \cos(\beta\pi y)}
 \end{aligned} \tag{107}$$

The numerical and analytical solutions of two-dimensional examples are present in Tables 16,17 with  $Re = 100$  and  $\tau = 5 \times 10^{-5}$ . The numerical solutions of the different time are presented in Figs. 10,11 with  $N \times N = 81 \times 81$ . From the Tables 16,17 and Figs. 12,13 of numerical simulation results, it can be seen that the proposed numerical scheme has high accuracy under the condition of large Reynolds number ( $Re = 100, 200, 500$ ). It is observed that the numerical solutions show great agreement with the analytical solutions. The Figs. 10,11 exhibit that the numerical solution of partial regions becomes steeper and steeper as the increase of time. This physical phenomenon validates the fact that the numerical solution is capable of describing shock wave. Moreover, note that Tables 16,17 and Figs. 10,11 indicate the property (the boundary condition (34)) of the solution of the two-dimensional Burgers' equation. The physical phenomena depicted in the Figs. 10,11 are analogical to those in Refs. [12, 44, 45, 46].

Table 16: Comparison with the proposed scheme and the analytical solutions of different coordinate positions  $(x, y)$  with  $Re = 100$ , at  $t = 0.25, 0.5$  for Example 7.

| $(x, y)$     | $t = 0.25$              |                    | $t = 0.5$               |                    |
|--------------|-------------------------|--------------------|-------------------------|--------------------|
|              | Analytical solution[12] | proposed scheme    | Analytical solution[12] | proposed scheme    |
| (0.25, 0.25) | 0.3935490117704355      | 0.393549011771103  | 0.2911828920816955      | 0.291182892082807  |
| (0.50, 0.25) | 0.6861822403861596      | 0.686182243447071  | 0.5605467081571704      | 0.560546708625940  |
| (0.75, 0.25) | 0.3935490117704355      | 0.393524523103096  | 0.2911828920816955      | 0.291180266677443  |
| (0.25, 0.50) | 0.2619506158413131      | 0.261950614753384  | 0.2619829318741635      | 0.261982931825796  |
| (0.50, 0.50) | 3.433140255652116E-70   | 0                  | 6.648346088881589E-70   | 0                  |
| (0.75, 0.50) | -0.2619506158413131     | -0.261950614753467 | -0.2619829318741635     | -0.261982931825921 |
| (0.25, 0.75) | -0.3935490117704355     | -0.393513909760747 | -0.2911828920816955     | -0.291179204683133 |
| (0.50, 0.75) | -0.6861822403861596     | -0.686182243439029 | -0.5605467081571704     | -0.560546708617027 |
| (0.75, 0.75) | -0.3935490117704355     | -0.393549011774452 | -0.2911828920816955     | -0.291182892085496 |

Table 17: Comparison with the proposed scheme and the exact solutions of different coordinate positions of  $(x, y)$  with  $Re = 100$  and  $t = 0.75, 1.0$  for Example 7.

| $(x, y)$     | $t = 0.75$              |                    | $t = 1.0$               |                    |
|--------------|-------------------------|--------------------|-------------------------|--------------------|
|              | Analytical solution[12] | proposed scheme    | Analytical solution[12] | proposed scheme    |
| (0.25, 0.25) | 0.2273774661403168      | 0.227377466141544  | 0.1858035619888798      | 0.185803561989915  |
| (0.50, 0.25) | 0.4479960634879613      | 0.447996063594949  | 0.3687873026249988      | 0.368787302662550  |
| (0.75, 0.25) | 0.2273774661403168      | 0.227377282040238  | 0.1858035619888798      | 0.185803538891363  |
| (0.25, 0.50) | 0.2180447995061038      | 0.218044799502132  | 0.1818603555820653      | 0.181860355581896  |
| (0.50, 0.50) | 2.301061067978292E-70   | 0                  | 7.783304094972026E-71   | 0                  |
| (0.75, 0.50) | -0.2180447995061038     | -0.218044799502212 | -0.1818603555820653     | -0.181860355581938 |
| (0.25, 0.75) | -0.2273774661403168     | -0.227377196569641 | -0.1858035619888798     | -0.185803526285714 |
| (0.50, 0.75) | -0.4479960634879613     | -0.447996063584584 | -0.3687873026249988     | -0.368787302652006 |
| (0.75, 0.75) | -0.2273774661403168     | -0.227377466144151 | -0.1858035619888798     | -0.185803561992506 |

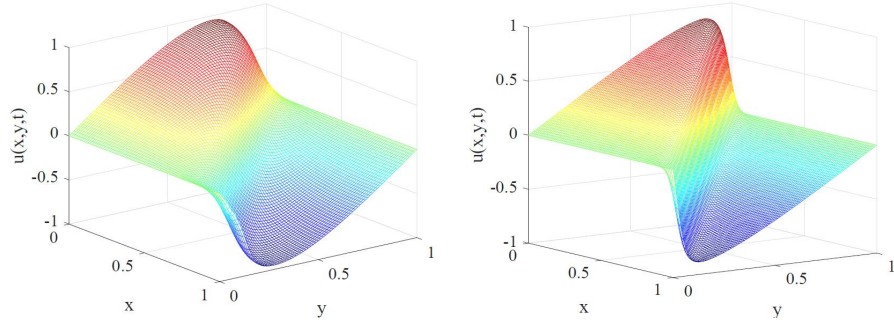


Figure 10: The numerical solution of the two-dimensional Burgers' equation for  $Re = 100$  at  $t = 0.25$  (Left) and  $t = 0.5$  (Right) with  $N \times N = 81 \times 81$  for Example 7.

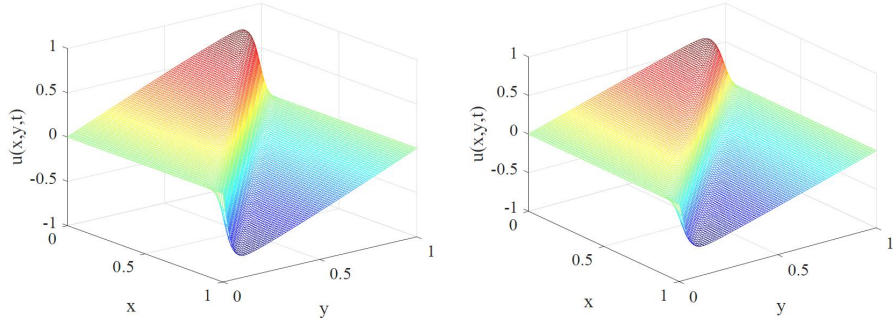


Figure 11: The numerical solution of the two-dimensional Burgers' equation for  $Re = 100$  at  $t = 0.5$  (Left) and  $t = 1.0$  (Right) with  $N \times N = 81 \times 81$  for Example 7.

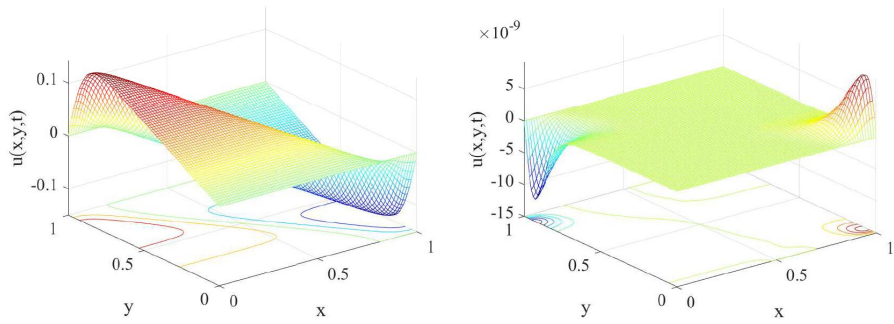


Figure 12: The numerical solution (Left) and the error (Right) of the two-dimensional Burgers' equation for  $Re = 200$  at  $t = 5.0$  with  $N \times N = 81 \times 81$  for Example 7.



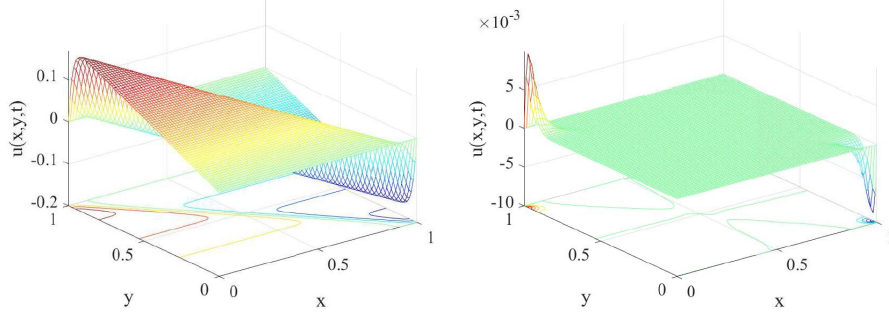


Figure 13: The numerical solution (Left) and the error (Right) of the two-dimensional Burgers' equation for  $Re = 500$  at  $t = 5.0$  with  $N \times N = 81 \times 81$  for Example 7.

**Example 8.** In order to test the applicability of the proposed scheme for multi-dimensional problems, we consider the three-dimensional Burgers' equations (7) over a square domain  $[0, 1] \times [0, 1] \times [0, 1]$ , with the initial conditions

$$\begin{cases} u(x, y, z, 0) = \frac{-2}{Re} \frac{\cos \pi x \sin \pi y \sin \pi z}{1 + \sin \pi x \sin \pi y \sin \pi z} \\ v(x, y, z, 0) = \frac{-2}{Re} \frac{\sin \pi x \cos \pi y \sin \pi z}{1 + \sin \pi x \sin \pi y \sin \pi z} \\ w(x, y, z, 0) = \frac{-2}{Re} \frac{\sin \pi x \sin \pi y \cos \pi z}{1 + \sin \pi x \sin \pi y \sin \pi z} \end{cases}, (x, y, z) \in \partial\Omega \quad (108)$$

The analytical solution for this problem is given by

$$\begin{cases} u = \frac{-2}{Re} \frac{\exp(-3\pi^2 \omega t) \cos \pi x \sin \pi y \sin \pi z}{1 + \exp(-3\pi^2 \omega t) \sin \pi x \sin \pi y \sin \pi z} \\ v = \frac{-2}{Re} \frac{\exp(-3\pi^2 \omega t) \sin \pi x \cos \pi y \sin \pi z}{1 + \exp(-3\pi^2 \omega t) \sin \pi x \sin \pi y \sin \pi z} \\ w = \frac{-2}{Re} \frac{\exp(-3\pi^2 \omega t) \sin \pi x \sin \pi y \cos \pi z}{1 + \exp(-3\pi^2 \omega t) \sin \pi x \sin \pi y \sin \pi z} \end{cases}, (x, y, z) \in \partial\Omega, t > 0 \quad (109)$$

The boundary conditions are extracted from the analytical solution. It is observed that the numerical solutions present great agreement with the analytical solutions. The slices of the four-dimensional images are used for observing three-dimensional Burgers' equations, which are depicted in Figs. 14,15,16. Figs. 17,18 present the numerical solutions and the errors between the exact solutions and the numerical solutions at  $t = 1$  with  $z = 0.25$  and  $Re = 100, 1000$ . The numerical results of this example show that the CFD-PIM-SMM scheme base on Hopf-Cole transformation is a numerical method with high precision and high efficiency for solving n-dimensional Burgers' system. The compari-

son is done with solutions obtained by the numerical solutions and the exact solutions for the three-dimensional Burgers' equations, which is presented in on left-hand side Figs. 17,18. All numerical figures of this example show that the proposed scheme has excellent accuracy and efficiency. Figs. 17,18 exhibit that the numerical solution of partial regions becomes steeper and steeper as  $Re = 100 \rightarrow 1000$ . This physical phenomenon validates the fact that the numerical solution is capable of describing shock wave.

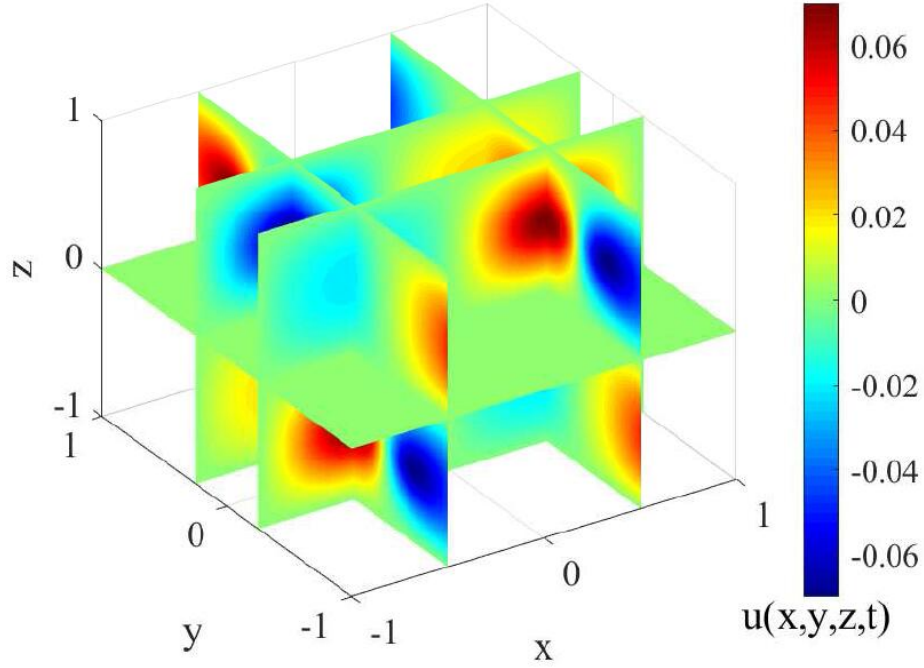


Figure 14: The slices of the four-dimensional figure of the solutions of the three-dimensional problem for the CFD-PIM-SSM scheme with spatial step size  $h_x = h_y = h_z = 1.25 \times 10^{-2}$  and time step size  $\tau = 5 \times 10^{-5}$  and  $Re = 100$  at  $t = 1$  for Example 8.

**Example 9.** We consider the system of three-dimensional Burgers' equation (6) in Sec.2.2.3, over a square domain  $[0, 1] \times [0, 1] \times [0, 1]$ , with the initial and

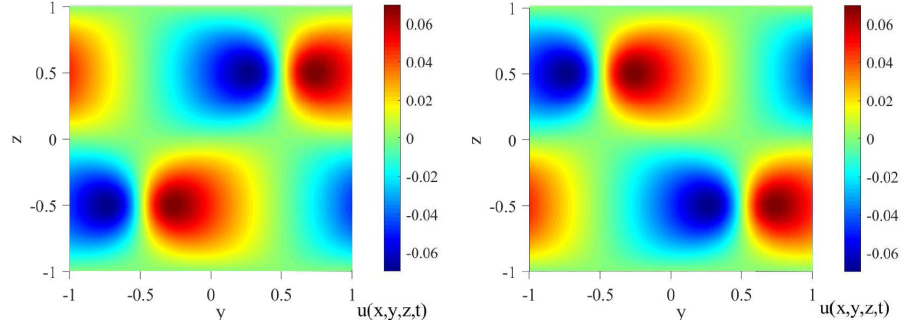


Figure 15: The slices of four-dimensional figures of the solution of the three-dimensional problem with  $x = -0.5$  (Left) and  $x = 0.5$  (Right) for Example 8.

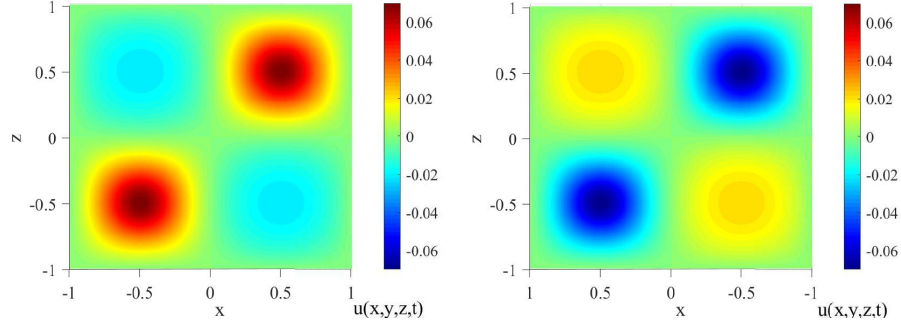


Figure 16: The slices of four-dimensional figures of the solution of the three-dimensional problem with  $y = -0.25$  (Left) and  $y = 0.25$  (Right) for Example 8.

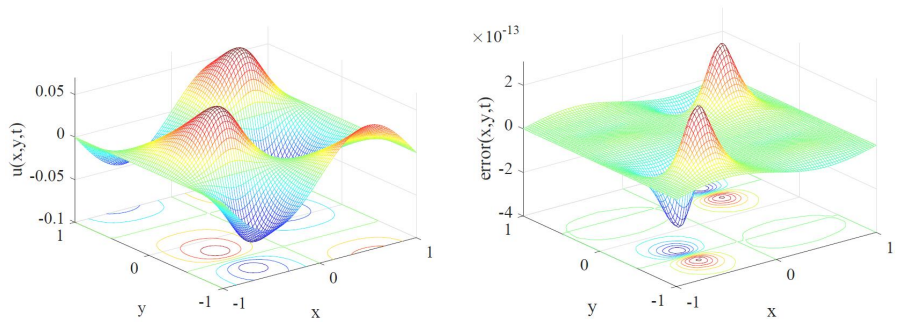


Figure 17: The three-dimensional figures of the solution (Left) and the error (Right) of the three-dimensional problem with  $z = 0.25$  and  $Re = 100$  at  $t = 1$  for Example 8.

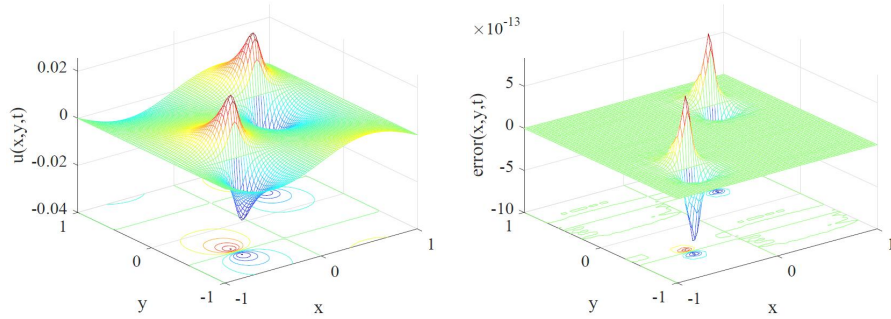


Figure 18: The three-dimensional figures of the solution (Left) and the error (Right) of the three-dimensional problem with  $z = 0.25$  and  $Re = 1000$  at  $t = 1$  for Example 8.

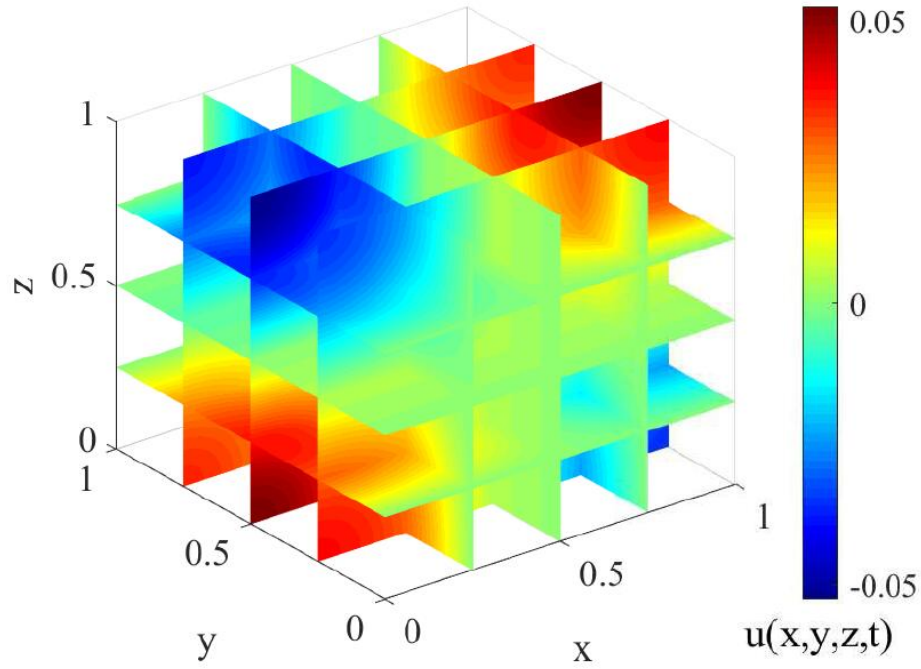


Figure 19: The slices of the four-dimensional figure of the solutions of the three-dimensional problem for the CFD-PIM-SSM scheme with spatial step size  $h_x = h_y = h_z = 1.25 \times 10^{-2}$  and time step size  $\tau = 5 \times 10^{-5}$  and  $Re = 10$  at  $t = 1$  for Example 9.

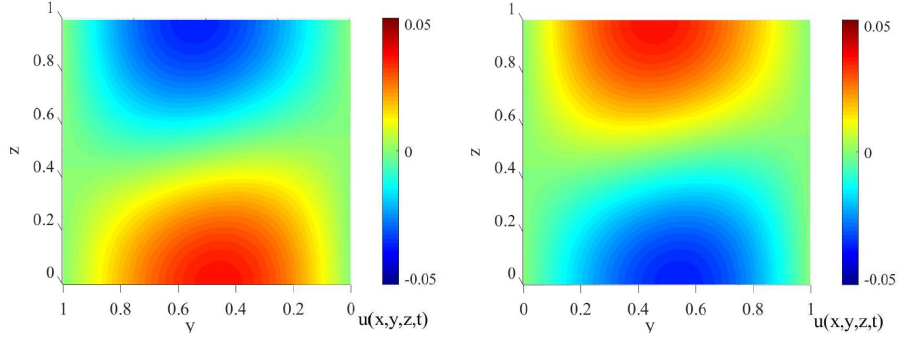


Figure 20: The slices of four-dimensional figures of the solution of the three-dimensional problem with  $x = 0.25$  (Left) and  $x = 0.75$  (Right) for Example 9.

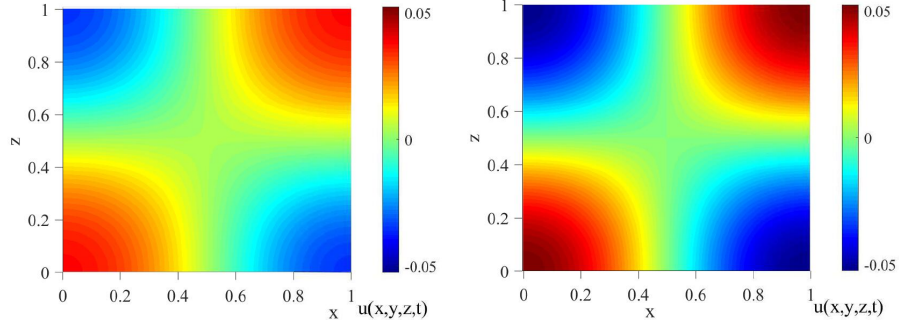


Figure 21: The slices of four-dimensional figures of the solution of the three-dimensional problem with  $y = 0.25$  (Left) and  $y = 0.5$  (Right) for Example 9.

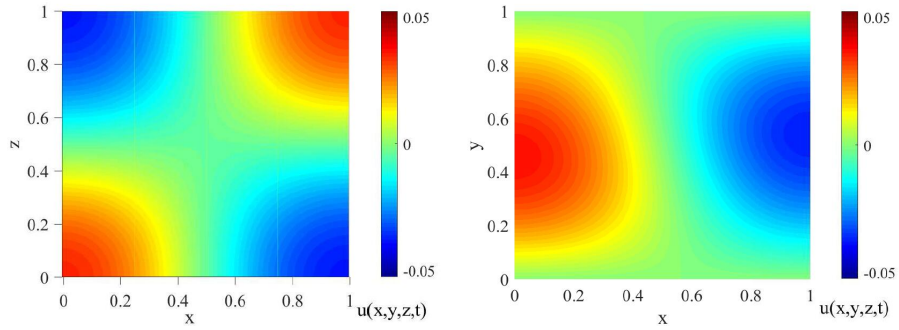


Figure 22: The slices of four-dimensional figures of the solution of the three-dimensional problem with  $y = 0.75$  (Left) and  $z = 0.25$  (Right) for Example 9.

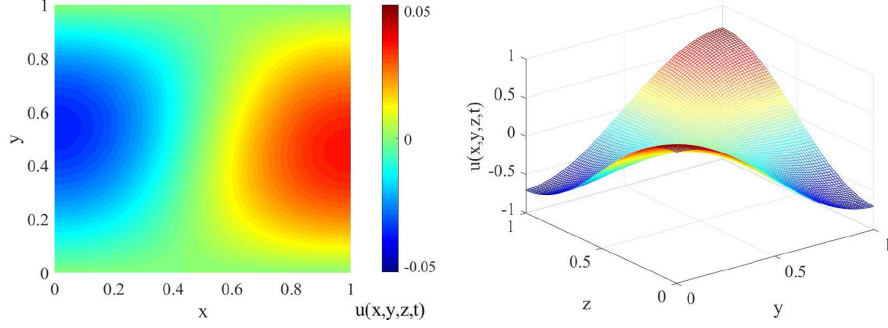


Figure 23: The slices of four-dimensional figures of the solution of the three-dimensional problem with  $z = 0.75$  (Left) and the numerical solution of the three-dimensional Burgers' equation at  $t = 0$  (Right) with  $N \times N = 81 \times 81$ ,  $x = 0.25$  and  $Re = 10$  for Example 9.

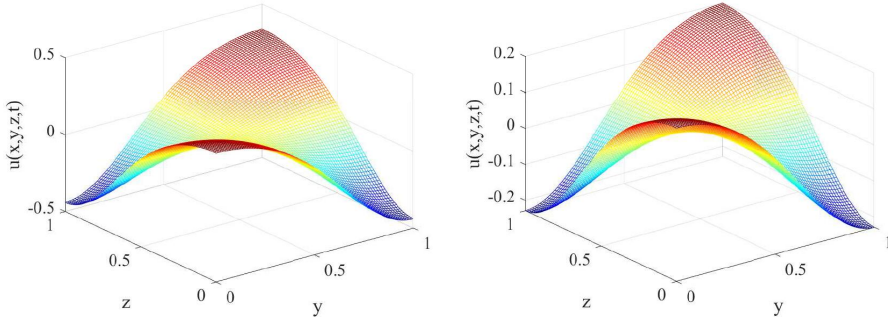


Figure 24: The numerical solution of the three-dimensional Burgers' equation at  $t = 0.2$  (Left) and  $t = 0.4$  (Right) with  $N \times N = 81 \times 81$ ,  $x = 0.25$  and  $Re = 10$  for Example 9.

boundary conditions (41,42), and the analytical solution

$$\begin{aligned}
 u(x, y, z, t) &= 2\pi\omega \frac{\sum_{\alpha, \beta, \gamma=0}^{\infty} \alpha C_{\alpha\beta\gamma} \exp[-(\alpha^2 + \beta^2 + \gamma^2)\pi^2\omega t] \sin(\alpha\pi x) \cos(\beta\pi y) \cos(\gamma\pi z)}{\sum_{\alpha, \beta, \gamma=0}^{\infty} C_{\alpha\beta\gamma} \exp[-(\alpha^2 + \beta^2 + \gamma^2)\pi^2\omega t] \cos(\alpha\pi x) \cos(\beta\pi y) \cos(\gamma\pi z)} \\
 v(x, y, z, t) &= 2\pi\omega \frac{\sum_{\alpha, \beta, \gamma=0}^{\infty} \beta C_{\alpha\beta\gamma} \exp[-(\alpha^2 + \beta^2 + \gamma^2)\pi^2\omega t] \cos(\alpha\pi x) \sin(\beta\pi y) \cos(\gamma\pi z)}{\sum_{\alpha, \beta, \gamma=0}^{\infty} C_{\alpha\beta\gamma} \exp[-(\alpha^2 + \beta^2 + \gamma^2)\pi^2\omega t] \cos(\alpha\pi x) \cos(\beta\pi y) \cos(\gamma\pi z)} \\
 w(x, y, z, t) &= 2\pi\omega \frac{\sum_{\alpha, \beta, \gamma=0}^{\infty} \gamma C_{\alpha\beta\gamma} \exp[-(\alpha^2 + \beta^2 + \gamma^2)\pi^2\omega t] \cos(\alpha\pi x) \cos(\beta\pi y) \sin(\gamma\pi z)}{\sum_{\alpha, \beta, \gamma=0}^{\infty} C_{\alpha\beta\gamma} \exp[-(\alpha^2 + \beta^2 + \gamma^2)\pi^2\omega t] \cos(\alpha\pi x) \cos(\beta\pi y) \cos(\gamma\pi z)}
 \end{aligned} \tag{110}$$

In order to verify the validity and practicability of the proposed scheme of



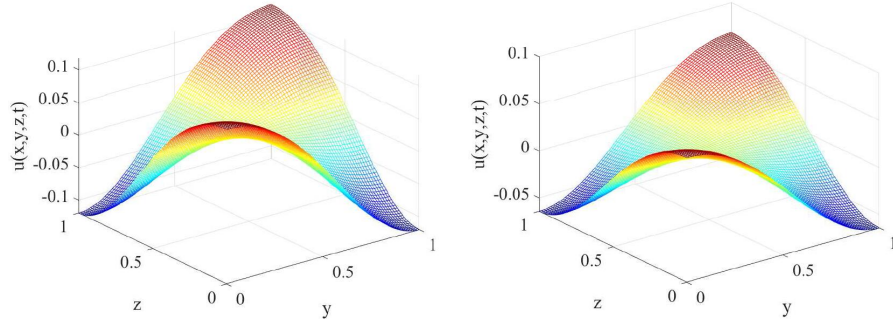


Figure 25: The numerical solution of the three-dimensional Burgers' equation at  $t = 0.6$  (Left) and  $t = 0.8$  (Right) with  $N \times N = 81 \times 81$ ,  $x = 0.25$  and  $Re = 10$  for Example 9.

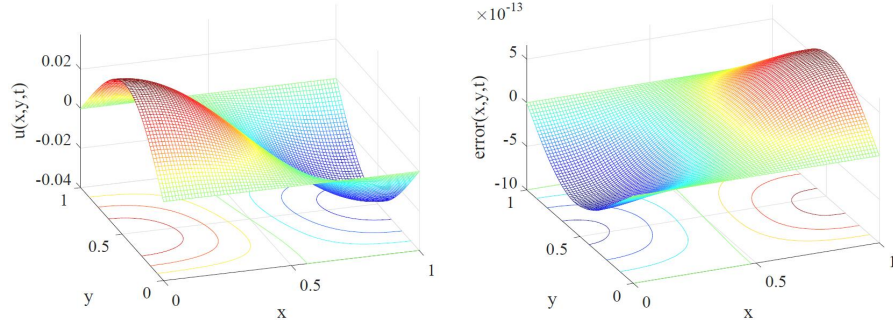


Figure 26: The three-dimensional figures of the solution (Left) and the error (Right) between the numerical and analytical solutions of the three-dimensional problem with  $z = 0.25$  and  $Re = 10$  at  $t = 1$  for Example 9.

three-dimensional Burgers' equation, the numerical solution is compared with the analytical solution. The numerical solution of the three-dimensional Burgers' equation (12) is given by the three-dimensional Hopf-Cole transformation (46). The correctness of the numerical solution of the heat conduction equation ensures the correctness of the numerical solution of the Burgers' equation. The higher the accuracy of numerical solution of the heat conduction equation, the higher the accuracy of the numerical solution of the Burgers' equation will be. The numerical and analytical solutions of the three-dimensional heat conduction equation are presented in Table 18 with  $Re = 10$  and  $\tau = 5 \times 10^{-5}$ . From the

Table 18: The solutions of the three-dimensional heat conduction equation with  $Re = 10$  at  $t = 0.1$  for Example 9. (The spatial step sizes of the FEM are  $h_x = h_y = h_z = 10^{-2}$ )

| $(x, y, z)$        | $\phi(x, y, z, t)$      |                     |                    |
|--------------------|-------------------------|---------------------|--------------------|
|                    | Analytical solution[12] | FEM[12]             | proposed scheme    |
| (0.25, 0.00, 0.00) | 0.5121139094268445      | 0.5121574025971580  | 0.5121122211115770 |
| (0.25, 0.25, 0.00) | 0.4021754605524777      | 0.4021832308799626  | 0.402175090853434  |
| (0.25, 0.25, 0.25) | 0.3332558679440735      | 0.3332624499504631  | 0.333255848934007  |
| (0.25, 0.50, 0.00) | 0.2221335878372145      | 0.2221195126283573  | 0.222134351589450  |
| (0.25, 0.50, 0.25) | 0.2145599507332575      | 0.2145578143852998  | 0.214560278902764  |
| (0.25, 0.75, 0.00) | 0.1232224673074507      | 0.1232115116009095  | 0.123222177969065  |
| (0.50, 0.00, 0.00) | 0.2350307713064107      | 0.2349996700538997  | 0.235032545451199  |
| (0.50, 0.25, 0.00) | 0.2221335878372145      | 0.2221195160032975  | 0.222134351729473  |
| (0.50, 0.25, 0.25) | 0.2145599507332575      | 0.2145578324085150  | 0.214560278977476  |
| (0.75, 0.00, 0.00) | 0.09757645937131027     | 0.09756832939249252 | 0.0975749310522441 |
| (0.75, 0.25, 0.00) | 0.1232224673074507      | 0.1232114495876140  | 0.123222177969033  |

Table 18 of numerical simulation results, it is observable that the numerical solutions present excellent consistency with the analytical solutions. The slices of the four-dimensional images are used for observing three-dimensional Burgers' equation, which are depicted in Figs. 20,21,22,23,24. The numerical solutions of the different time are presented in Figs. 23,24,25 with  $N \times N \times N = 81 \times 81 \times 81$ . It can be observed from Figs. 23,24,25 when  $Re = 10$ , the numerical solution of the Burgers' equation will generate shock wave. This physical phenomenon validates the fact that the numerical solution is capable of describing shock wave. The physical phenomena depicted in the Figs. 23,24,25 are similar to those in Ref.[12]. We make a three-dimensional Burgers' equation with numerical solutions and errors in Fig. 26. It is observed that the numerical solution is very consistent with the analytical solution.

## 6. Conclusion

This paper proposed modified Hopf-Cole transformation for n-dimensional Burgers' system. After obtaining the n-dimensional heat conduction equations, we present a new high-order exponential time differencing precise integration method schemes in combination with the sixth-order compact finite difference



scheme, which have been developed for the numerical solutions of n-dimensional heat conduction equations. The proposed scheme is tested on night examples and the results are entirely satisfactory in comparison with the analytical solutions. The findings can be summarized as follows

- (1) For the examples of the ordinary initial and boundary conditions, the solutions can describe shock wave phenomena for large Reynolds numbers ( $Re \geq 1000$ ), which is characterized by high precision and high efficiency.
- (2) For the complicated initial and boundary conditions problems, the proposed scheme obtains excellent accuracy and high efficiency in comparison to the other numerical techniques available in the Refs. [5, 11, 38, 40, 41, 42, 43, 53, 54, 56, 57].
- (3) After the modification of Hopf-Cole transformation and optimization of computer programming, the present scheme has commendable adaptability and high efficiency in the calculation examples.
- (4) It is found that the proposed results are in good agreement with the analytical solutions for two-dimensional and three-dimensional problems. This scheme includes linear problems and nonlinear problems, which can be easily extended to solve model equations of high-dimensional problems.

### Acknowledgement

This work is financially supported by the National Natural Science Foundation of China(No. 11826208).

### References

### References

- [1] H. BATEMAN, Some recent researches on the motion of fluids, Monthly Weather Review 43 (4) (1915) 163–170. doi:10.1175/1520-0493(1915)43<163:SRR0TM>2.0.CO;2.

- [2] J. A. S. e. J. M. Burgers (auth.), F. T. M. Nieuwstadt, Selected Papers of J. M. Burgers, 1st Edition, Springer Netherlands, 1995.
- [3] J. Burgers, A mathematical model illustrating the theory of turbulence, Vol. 1 of Advances in Applied Mechanics, Elsevier, 1948, pp. 171 – 199. doi:[https://doi.org/10.1016/S0065-2156\(08\)70100-5](https://doi.org/10.1016/S0065-2156(08)70100-5).
- [4] N. J. Zabusky, M. D. Kruskal, Interaction of "solitons" in a collisionless plasma and the recurrence of initial states , Physical Review Letters 15 (6) (1965) 240–243.
- [5] H. R. Y. Kaysar.Rahman, Nurmamat, Some New Semi-Implicit Finite Difference Schemes for Numerical Solution of Burgers Equation, International Conference on Computer Application and System Modeling (1) 63–75. doi:[10.1007/s00244-017-0417-6](https://doi.org/10.1007/s00244-017-0417-6).
- [6] E. Hopf, The partial differential equation  $u_t + u u_x = \mu x x$ , Communications on Pure and Applied Mathematics 3 (3) (1950) 201–230. doi:[10.1002/cpa.3160030302](https://doi.org/10.1002/cpa.3160030302).
- [7] J. D. Cole, On a quasilinear parabolic equations occurring in aerodynamics, Quart. Appl. Math. 9 (2) (1951) 225–236. doi:[10.1090/qam/42889](https://doi.org/10.1090/qam/42889).
- [8] M. Kumar, S. Pandit, A composite numerical scheme for the numerical simulation of coupled Burgers' equation, Computer Physics Communications 185 (3) (2014) 809–817. doi:[10.1016/j.cpc.2013.11.012](https://doi.org/10.1016/j.cpc.2013.11.012).
- [9] H. Brezis, F. Browder, Partial differential equations in the 20th century, Advances in Mathematics 135 (1) (1998) 76 – 144. doi:<https://doi.org/10.1006/aima.1997.1713>.
- [10] U. Frisch, J. Bec, Burgulence, Springer Berlin Heidelberg, Berlin, Heidelberg, 2001, pp. 341–383. doi:[10.1007/3-540-45674-0\\_7](https://doi.org/10.1007/3-540-45674-0_7). URL [https://doi.org/10.1007/3-540-45674-0\\_7](https://doi.org/10.1007/3-540-45674-0_7)

- [11] H. P. Bhatt, A. Q. Khaliq, Fourth-order compact schemes for the numerical simulation of coupled Burgers' equation, *Computer Physics Communications* 200 (2016) 117–138. doi:10.1016/j.cpc.2015.11.007. URL <http://dx.doi.org/10.1016/j.cpc.2015.11.007>
- [12] Q. Gao, M. Y. Zou, An analytical solution for two and three dimensional nonlinear Burgers' equation, *Applied Mathematical Modelling* 45 (2016) 255–270. doi:10.1016/j.apm.2016.12.018.
- [13] A. H. Khater, R. S. Temsah, M. M. Hassan, A Chebyshev spectral collocation method for solving Burgers'-type equations, *Journal of Computational and Applied Mathematics* 222 (2) (2008) 333–350. doi:10.1016/j.cam.2007.11.007.
- [14] R. C. Mittal, G. Arora, Numerical solution of the coupled viscous Burgers' equation, *Communications in Nonlinear Science and Numerical Simulation* 16 (3) (2011) 1304–1313. doi:10.1016/j.cnsns.2010.06.028.
- [15] H. M. Jaradat, M. Syam, M. Alquran, S. Al Shara, K. M. Abohassn, A new two-mode coupled Burgers equation: Conditions for multiple kink solution and singular kink solution to exist, *Ain Shams Engineering Journal* 9 (4) (2018) 3239–3244. doi:10.1016/j.asej.2017.12.005.
- [16] C. H. Chan, M. Czubak, Regularity of solutions for the critical N-dimensional Burgers' equation, *Annales de l'Institut Henri Poincaré (C) Analyse Non Linéaire* 27 (2) (2010) 471–501. arXiv:arXiv:0810.3055v3, doi:10.1016/j.anihpc.2009.11.008.
- [17] Y. Chen, E. Fan, M. Yuen, The Hopf-Cole transformation, topological solitons and multiple fusion solutions for the n-dimensional Burgers system, *Physics Letters, Section A: General, Atomic and Solid State Physics* 380 (1-2) (2016) 9–14. doi:10.1016/j.physleta.2015.09.033.
- [18] M. Wang, J. Zhang, X. Li, N-dimensional Auto-Bäcklund transformation and exact solutions to n-dimensional Burgers system, *Applied Mathematics*

- Letters 63 (2017) 46–52. [arXiv:1607.07208](#), [doi:10.1016/j.aml.2016.07.019](#).
- [19] F. D. Andrea, R. Vautard, Extratropical low-frequency variability as a low-dimensional problem I: A simplified model, *Quarterly Journal of the Royal Meteorological Society* 127 (574) (2001) 1357–1374. [doi:10.1256/smsqj.57412](#).
- [20] J. E. Marsden, L. Sirovich, S. S. Antman, G. Iooss, P. Holmes, D. Barkley, M. Dellnitz, P. Newton, *Texts in Applied Mathematics 2, Mechanics and Symmetry* 17. [doi:10.1016/j.smr.2017.10.004](#).
- [21] J. Li, Y.-T. Chen, *Computational Partial Differential Equations Using MATLAB*, 2008. [doi:10.1201/9781420089059](#).
- [22] S. C. R. Dennis, J. D. Hudson, Compact h4 finite-difference approximations to Operators of Navier-Stokes Type, *Journal of Computational Physics* 85 (2) (1989) 390–416. [doi:https://doi.org/10.1016/0021-9991\(89\)90156-3](#).  
URL <http://www.sciencedirect.com/science/article/pii/S0021999189901563>
- [23] S. K. Lele, Compact finite difference schemes with spectral-like resolution, *Journal of Computational Physics* 103 (1) (1992) 16–42. [arXiv:fld.1](#), [doi:10.1016/0021-9991\(92\)90324-R](#).
- [24] J. Zhao, Compact finite difference methods for high order integro-differential equations, *Applied Mathematics and Computation* 221 (2013) 66–78. [doi:https://doi.org/10.1016/j.amc.2013.06.030](#).  
URL <http://www.sciencedirect.com/science/article/pii/S0096300313006450>
- [25] M. C. Lai, J. M. Tseng, A formally fourth-order accurate compact scheme for 3D Poisson equation in cylindrical coordinates, *Journal of Computa-*

- tional and Applied Mathematics 201 (1) (2007) 175–181. doi:10.1016/j.cam.2006.02.011.
- [26] T. Nihei, K. Ishii, A fast solver of the shallow water equations on a sphere using a combined compact difference scheme, Journal of Computational Physics 187 (2) (2003) 639–659. doi:[https://doi.org/10.1016/S0021-9991\(03\)00152-9](https://doi.org/10.1016/S0021-9991(03)00152-9).  
URL <http://www.sciencedirect.com/science/article/pii/S0021999103001529>
- [27] G. Sutmann, Compact finite difference schemes of sixth order for the Helmholtz equation, Journal of Computational and Applied Mathematics 203 (1) (2007) 15–31. doi:10.1016/j.cam.2006.03.008.
- [28] X. Wang, Z. F. Yang, G. H. Huang, High-order compact difference scheme for convection-diffusion problems on nonuniform grids, Journal of Engineering Mechanics-Asce 131 (12) (2005) 1221–1228. doi:10.1061/(asce)0733-9399(2005)131:12(1221).
- [29] V. Kumar, High-order compact finite-difference scheme for singularly-perturbed reaction-diffusion Problems on a new mesh of Shishkin type, Journal of Optimization Theory and Applications 143 (1) (2009) 123–147. doi:10.1007/s10957-009-9547-y.
- [30] M. Mehra, K. S. Patel, Algorithm 986, ACM Transactions on Mathematical Software 44 (2) (2017) 1–31. doi:10.1145/3119905.  
URL <http://dl.acm.org/citation.cfm?doid=3132683.3119905>
- [31] S. Sen, Fourth order compact schemes for variable coefficient parabolic problems with mixed derivatives, Computers & Fluids 134-135 (2016) 81–89. doi:<https://doi.org/10.1016/j.compfluid.2016.05.002>.  
URL <http://www.sciencedirect.com/science/article/pii/S0045793016301384>

- [32] C. Moler, C. Van Loan, Nineteen Dubious Ways to Compute the Exponential of a Matrix, Twenty-Five Years Later, SIAM Review 45 (1) (2003) 3–49. [arXiv:arXiv:1011.1669v3](#), [doi:10.1137/S00361445024180](#).
- [33] Z. Wan-Xie, On precise integration method, Journal of Computational and Applied Mathematics 163 (1) (2004) 59–78. [doi:10.1016/j.cam.2003.08.053](#).
- [34] Q. Zhang, C. Zhang, L. Wang, The compact and Crank-Nicolson ADI schemes for two-dimensional semilinear multidelay parabolic equations, Journal of Computational and Applied Mathematics 306 (2016) 217–230. [doi:10.1016/j.cam.2016.04.016](#).
- [35] S. Karaa, J. Zhang, High order ADI method for solving unsteady convection-diffusion problems, Journal of Computational Physics 198 (1) (2004) 1–9. [doi:10.1016/j.jcp.2004.01.002](#).
- [36] S. Journal, A. Mathematics, N. Mar, The Numerical Solution of Parabolic and Elliptic Differential Equations Author ( s ): D . W . Peaceman and H . H . Rachford , Jr . Published by : Society for Industrial and Applied Mathematics Stable URL : <http://www.jstor.org/stable/2098834> . 3 (1) (2013) 28–41.
- [37] Gilbert, On the Construction and Comparison of Difference Schemes Author ( s ): Gilbert Strang Source : SIAM Journal on Numerical Analysis , Vol . 5 , No . 3 ( Sep . , 1968 ), pp . 506-517 Published by : Society for Industrial and Applied Mathematics Stable URL : [h](#), Society 5 (3) (2013) 506–517.
- [38] M. K. Kadalbajoo, A. Awasthi, A numerical method based on Crank-Nicolson scheme for Burgers’ equation, Applied Mathematics and Computation 182 (2) (2006) 1430–1442. [doi:10.1016/j.amc.2006.05.030](#).
- [39] V. Mukundan, A. Awasthi, Efficient numerical techniques for Burgers’

- equation, *Applied Mathematics and Computation* 262 (2015) 282–297. doi:10.1016/j.amc.2015.03.122.
- [40] R. Jiwari, A hybrid numerical scheme for the numerical solution of the Burgers’ equation, *Computer Physics Communications* 188 (2015) 59–67. doi:10.1016/j.cpc.2014.11.004.
- [41] R. Jiwari, A Haar wavelet quasilinearization approach for numerical simulation of Burgers’ equation, *Computer Physics Communications* 183 (11) (2012) 2413–2423. doi:10.1016/j.cpc.2012.06.009.
- [42] M. Seydaolu, An accurate approximation algorithm for Burgers’ equation in the presence of small viscosity, *Journal of Computational and Applied Mathematics* 344 (2018) 473–481. doi:10.1016/j.cam.2018.05.063. URL <https://doi.org/10.1016/j.cam.2018.05.063>
- [43] D. K. G. W. Wei, Distributed approximating functional approach to Burgers’ equation in one and two space dimensions, *Computer Physics Communications* 93 (109) (1998) 93–109. doi:10.1016/S0010-4655(98)00041-1.
- [44] X. H. Zhang, J. Ouyang, L. Zhang, Element-free characteristic Galerkin method for Burgers’ equation, *Engineering Analysis with Boundary Elements* 33 (3) (2009) 356–362. doi:10.1016/j.enganabound.2008.07.001.
- [45] L. Zhang, J. Ouyang, X. Wang, X. Zhang, Variational multiscale element-free Galerkin method for 2D Burgers’ equation, *Journal of Computational Physics* 229 (19) (2010) 7147–7161. doi:10.1016/j.jcp.2010.06.004. URL <http://dx.doi.org/10.1016/j.jcp.2010.06.004>
- [46] S. ul Islam, B. Šarler, R. Vertnik, G. Kosec, Radial basis function collocation method for the numerical solution of the two-dimensional transient nonlinear coupled Burgers’ equations, *Applied Mathematical Modelling* 36 (3) (2012) 1148–1160. doi:10.1016/j.apm.2011.07.050.

- [47] W. F. Perger, A. Bhalla, M. Nardin, A numerical evaluator for the generalized hypergeometric series, *Computer Physics Communications* 77 (2) (1993) 249–254. doi:10.1016/0010-4655(93)90008-Z.
- [48] W. X. Zhong, Combined method for the solution of asymmetric Riccati differential equations, *Computer Methods in Applied Mechanics and Engineering* 191 (1) (2001) 93–102. doi:https://doi.org/10.1016/S0045-7825(01)00246-8.
- [49] J. Zhang, Q. Gao, S. J. Tan, W. X. Zhong, A precise integration method for solving coupled vehicle-track dynamics with nonlinear wheel-rail contact, *Journal of Sound and Vibration* 331 (21) (2012) 4763–4773. doi:10.1016/j.jsv.2012.05.033.
- [50] M. F. Wang, F. T. Au, On the precise integration methods based on Padé approximations, *Computers and Structures* 87 (5-6) (2009) 380–390. doi:10.1016/j.compstruc.2008.11.004.
- [51] F. Zhou, Y. You, G. Li, G. Xie, G. Li, The precise integration method for semi-discretized equation in the dual reciprocity method to solve three-dimensional transient heat conduction problems, *Engineering Analysis with Boundary Elements* 95 (June) (2018) 160–166. doi:10.1016/j.enganabound.2018.07.005.
- [52] F. Han, W. Dai, New higher-order compact finite difference schemes for 1D heat conduction equations, *Applied Mathematical Modelling* 37 (16-17) (2013) 7940–7952. doi:10.1016/j.apm.2013.03.026.
- [53] R. C. Mittal, R. K. Jain, Numerical solutions of nonlinear Burgers’ equation with modified cubic B-splines collocation method, *Applied Mathematics and Computation* 218 (15) (2012) 7839–7855. doi:10.1016/j.amc.2012.01.059.
- [54] T. W. Sheu, C. F. Chen, L. W. Hsieh, Development of a sixth-order two-dimensional convection-diffusion scheme via Cole-Hopf transformation,



- Computer Methods in Applied Mechanics and Engineering 191 (27-28) (2002) 2979–2995. doi:10.1016/S0045-7825(02)00220-7.
- [55] D. Li, C. Zhang, M. Ran, A linear finite difference scheme for generalized time fractional Burgers equation, Applied Mathematical Modelling 40 (11-12) (2016) 6069–6081. doi:10.1016/j.apm.2016.01.043.
- [56] S. Kutluay, A. R. Bahadir, A. Özde, Numerical solution of one-dimensional Burgers equation: Explicit and exact-explicit finite difference methods, Journal of Computational and Applied Mathematics 103 (2) (1999) 251–261. doi:10.1016/S0377-0427(98)00261-1.
- [57] H. Lai, C. Ma, A new lattice Boltzmann model for solving the coupled viscous Burgers’ equation, Physica A: Statistical Mechanics and its Applications 395 (2014) 445–457. doi:10.1016/j.physa.2013.10.030.
- [58] S. Bak, P. Kim, D. Kim, A semi-Lagrangian approach for numerical simulation of coupled Burgers’ equations, Communications in Nonlinear Science and Numerical Simulation 69 (2019) 31–44. doi:10.1016/j.cnsns.2018.09.007.
- [59] W. Liao, A fourth-order finite-difference method for solving the system of two-dimensional burgers’ equations, International Journal for Numerical Methods in Fluids 64 (5). doi:10.1002/fluid.2163.